SANDIA REPORT

SAND2003-1151
Unlimited Release
Printed April 2003

Final Report:
CNC Micromachines LDRD #10793

Bernhard Jokiel, Jr., Gilbert L. Benavides, Lothar F. X. Bieg and James J. Allen

Prepared by
Sandia National Laboratories
Albuquerque, New Mexico 87185 and Livermore, California 94550

Sandia is a multiprogram laboratory operated by Sandia Corporation,
a Lockheed Martin Company, for the United States Department of Energy's
National Nuclear Security Administration under Contract DE-AC04-94AL85000.

Issued by Sandia National Laboratories, operated for the United States Department of Energy by Sandia Corporation.

Available to DOE and DOE contractors from
U.S. Department of Energy
Office of Scientific and Technical Information
P.O. Box 62
Oak Ridge, TN 37831

Telephone: (865)576-8401
Facsimile: (865)576-5728
E-Mail: reports@adonis.osti.gov
Online ordering: http://www.doe.gov/bridge

Available to the public from
U.S. Department of Commerce
National Technical Information Service
5285 Port Royal Rd
Springfield, VA 22161

Telephone: (800)553-6847
Facsimile: (703)605-6900
E-Mail: orders@ntis.fedworld.gov
Online order: http://www.ntis.gov/help/ordermethods.asp?loc=7-4-0#online

SAND2003-1151
Unlimited Release
Printed March 2003

Final Report:
CNC Micromachines LDRD #10793

Bernhard Jokiel, Jr., Gilbert Benavides and Lothar Bieg
Mechanical Engineering Department

James Allen
MEMS Device Technologies

Sandia National Laboratories
P.O. Box 5800
Albuquerque, NM 87185-0958

Abstract

The three-year LDRD "CNC Micromachines" was successfully completed at the end of FY02. The project had four major breakthroughs in spatial motion control in MEMS: (1) A unified method for designing scalable planar and spatial on-chip motion control systems was developed. The method relies on the use of parallel kinematic mechanisms (PKMs) that when properly designed provide different types of motion on-chip without the need for post-fabrication assembly, (2) A new type of actuator was developed – the linear stepping track drive (LSTD) that provides open loop linear position control that is scalable in displacement, output force and step size. Several versions of this actuator were designed, fabricated and successfully tested. (3) Different versions of XYZ translation only and PTT motion stages were designed, successfully fabricated and successfully tested demonstrating absolutely that on-chip spatial motion control systems are not only possible, but are a reality. (4) Control algorithms, software and infrastructure based on MATLAB were created and successfully implemented to drive the XYZ and PTT motion platforms in a controlled manner. The control software is capable of reading an M/G code machine tool language file, decode the instructions and correctly calculate and apply position and velocity trajectories to the motion devices linear drive inputs to position the device platform along the trajectory as specified by the input file. A full and detailed account of design methodology, theory and experimental results (failures and successes) is provided.

TABLE OF CONTENTS

This Page Intentionally Left Blank

1. Introduction

1.1. Project Purpose

The information contained herein are the findings of the CNC Micromachines LDRD, funded from fiscal years FY00 ($325k), FY01 ($225k) and FY02 ($325k).

The purpose of the CNC Micromachines LDRD was to investigate and develop a general capability for motion control on a silicon die that may be programmed or otherwise remotely electronically controlled to provide spatially controllable motion on a silicon chip. The capability generated was to be manufacturable using the SUMMiT-V process, flexible and adaptable to create different types of motion control (translation only, piston-tip-tilt, cylindrical, etc.), robust enough to carry (or scaled to carry) a load representative of something that is a constituent part (or tool used) in a micro assembled system and need very little or no assembly.

The team consisted of:

Bernhard Jokiel, Jr.	14184
Gilbert Benavides	14184
Lothar Bieg	14184
James Allen	01769

1.2. Report Overview

The rest of this report deals with theory, technical achievements, processes and outcomes of the LDRD project and is organized as follows:

Chapter 2 – Brief Overview of the SUMMiT-V process.
Chapter 3 – Motion Platform Design Requirements and Constraints
Chapter 4 – MEMS Linear Stepping Track Drives
Chapter 5 – XYC Planar Motion Platform
Chapter 6 – XYZ Translation Only Spatial Motion Platform
Chapter 7 – Piston-Tip-Tilt Spatial Motion Platform
Chapter 8 – Conclusion

2. Brief Overview of SUMMiT-V Process

SUMMiT-V™ stands for "Sandia's Ultra-planar Micro-Machining Technology" is a Sandia National Laboratories patented process for silicon surface micromachining. This process is used to create complex micro electric mechanisms (MEMS) in silicon using thin film deposition, patterning and etching techniques. While it is the layering process that generates the devices, it is the release process that frees the polysilicon devices from their silicon oxide support structure. The released die however are not useful until they are put into an electronic package and bonded to electrical leads. In the following sections are brief synopsizes of each of these steps. In a single fabrication run, up to eight unique designs may be built. Each design is called a module. Each module is 3mm x 6mm. Two or more modules may be put together and are called a concatenated module. If all eight modules are put together, a maximum die size of approximately 12mm x 12mm is created.

2.1. The SUMMiT-V Process Itself

SUMMiT-V™ consists of five layers of n-type polysilicon separated by sacrificial silicon oxide layers [1, 2]. The layers are built-up on a silicon-nitride coated, <100>, n-type, 6" silicon wafer substrate. Each layer may be patterned and etched into a geometry chosen by the device designer as is commonly done in integrated circuit production. This process of deposition, patterning and etching provides the means to create complex, interconnected, micro-mechanisms complete with motors and drive linkages containing spinning and translating elements with minimum feature sizes of 1μm. Figure 2-1 shows the series of steps of the SUMMiT-V™ process.

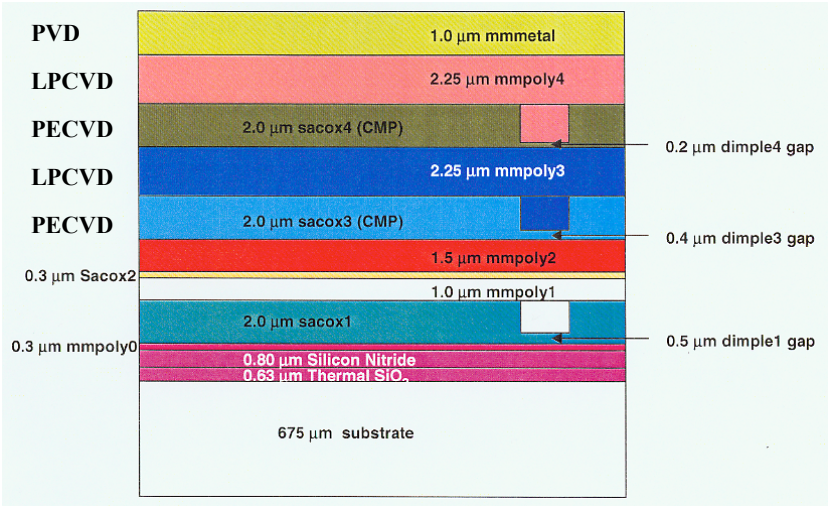

Figure 2-1 – Layers and processing steps involved during the SUMMiT-V™ process [1, 2].

Although there are five layers of polysilicon, there are really only four layers (Poly1-Poly4) that can be used to form structural elements (Figure 2-2). Poly0 provides a means for a ground plane, electrical wiring and connections, and a means to anchor the devices formed by the other four structural layers to the silicon substrate. Conformal structural layers Poly1 and Poly2 may be

laminated together to form a single layer, separated by SaxOx2 to form two separate structural layers, or connected together through a "pin joint cut" allowing the creation of free-spinning hubs for gears and rollers in Poly2. Each layer may be connected to the layer beneath by patterning and etching the SaxOx layer below.

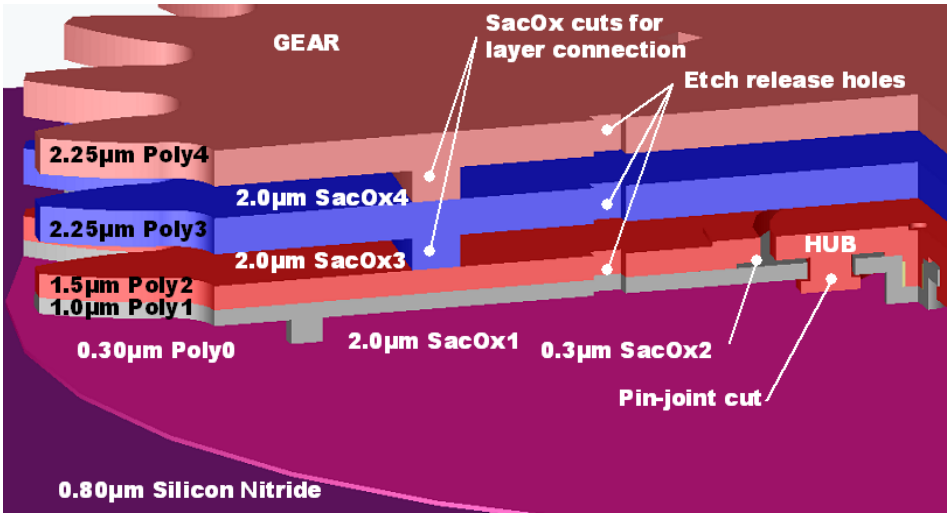

Figure 2-2 – Cross section of five level gear in SUMMiT-V™ [3].

2.2. Part release and coating

Once the fabrication process is complete, the silicon mechanisms are not useable until the silicon oxide "scaffolding" entrapping the silicon devices is removed. The release process, while sounding very simple, is actually a very tricky business. Only an overview of the process is described here. However much work has been done to examine the release process hazards and problem solutions in detail [4]. Figure 2-3 summarizes the release process steps.

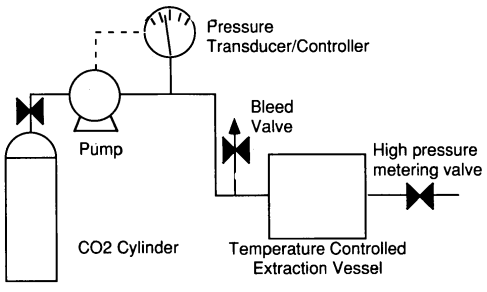

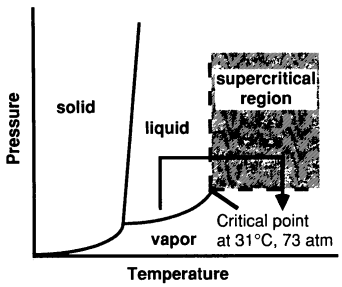

Process:
- **transfer samples to methanol**
- **place samples in vessel**
- **exchange methanol with supercritical CO_2**
- **vent vessel maintaining supercritical state**

Advantages:
- **initially free beam lengths up to 2000 µm!**

Disadvantages:
- **expensive apparatus**
- **safety concern - high pressure**
- **surface remains hydrophilic (if initially peroxide cleaned)**

Figure 2-3 – The release process [4].

To alleviate stiction and friction problems [5-28], a coating for MEMS was developed at Sandia National Laboratories [5-28]. This self-assembled monolayer coating applied by vapor deposition is commonly called a VSAM coating (Figure 2-4). During the span of this project both coated and uncoated devices were tested.

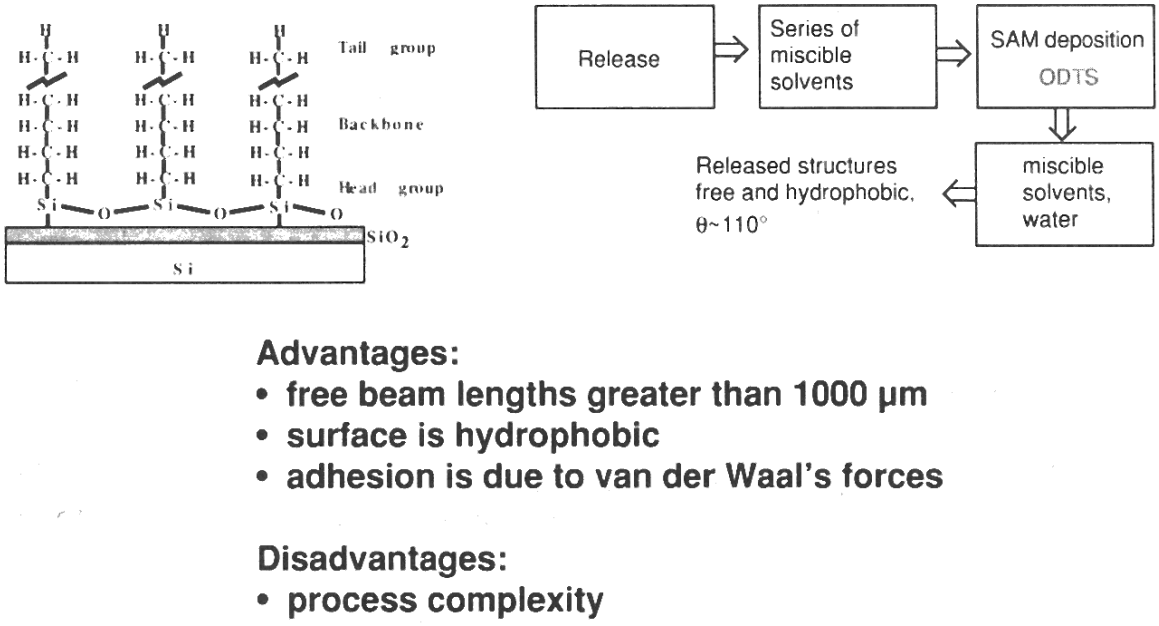

Figure 2-4 – VSAMs coating for SUMMiT-V™ MEMS devices [4].

2.3. Packaging

A MEMS device is not useable in the real world without being put in some sort of a package. The package not only serves to protect the device, but also provides electrical connections for drive and sensor signals on and off the chip. Figure 2-5 shows examples of different packaging solution for integrated MEMS devices.

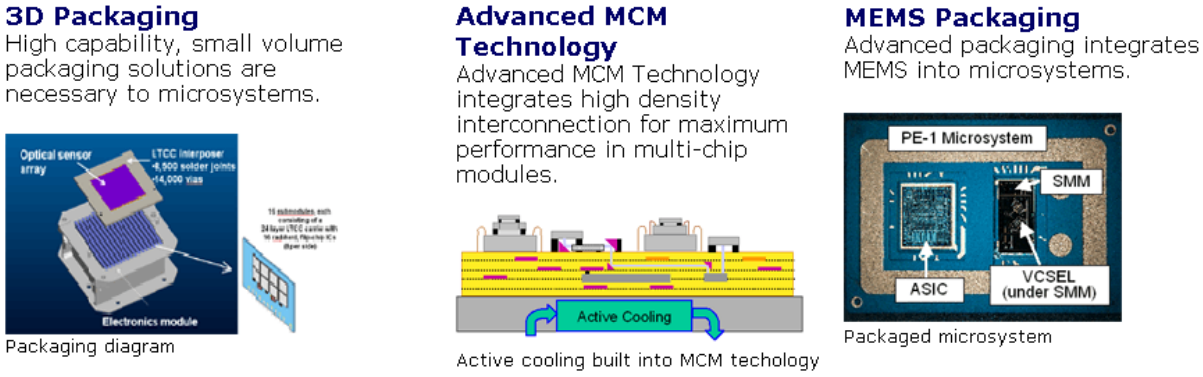

Figure 2-5 – Examples of packaging for integrated MEMS devices and electronics.

3.0 Motion Platform Design Requirements and Constraints

The purpose of the project was to develop a series of planar and spatial motion platforms that are fabricated in a planar position fully assembled. While planar platforms would be ready to actuate after release, the spatial mechanisms would be popped-up for deployment. There are many ways that this design problem may be approached. However there are two fundamentally different ways that a motion device may be constructed from serially connected links, or links connected in parallel (Figure 3-1).

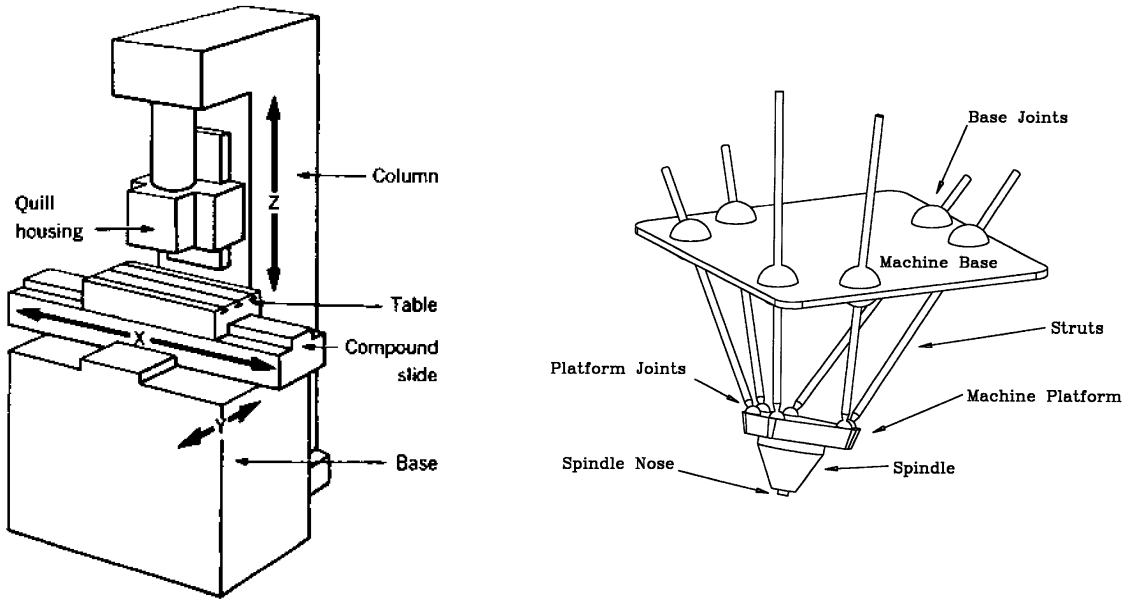

(a) **(b)**

Figure 3-1 – Machine architecture: (a) Serial linkages, (b) Parallel linkages.

Complicating this fundamental design choice is the desire to build a capability that will allow a MEMS mechanism designer to easily construct different on-chip spatial motion mechanisms specifically tailored to generate different types of motion (i.e. – XYZ translation only, piston-tip-tilt, planar XY motion, etc.) merely by changing joint type or placement. What is more is it is desirable to have a toolbox of parts (motors, joints and links) that may be arbitrarily joined to build such mechanisms.

Further complicating this design problem is the need to work within the constraints of the SUMMiT-V™ process using only four structural layers of polysilicon with the additional constraint that all of the polysilicon is conductive. Table 3-1 summarizes the design constraints put on the mechanism construction.

Table 3-1 – Design constraints for constructing planar and spatial motion devices using the SUMMiT-V™ process.

Constraint	Reason
All constituent parts must be 2D and planar.	Fabrication process is planar.
All constituent parts must be fully assembled and interconnected during the fabrication process.	Constituent parts are very small. Assembly step is very difficult and therefore undesirable.
Constituent parts must be able to be connected to one another in an arbitrary order.	Allows a great deal of mechanism design flexibility.
A large number of device designs must be enabled from a small finite number of parts or building blocks.	Increases design flexibility and speed. Limits the amount of engineering and design time required.
Stacked actuators must be avoided to prevent cross talk between axis command signals.	All of the polysilicon is conductive and there are no insulating layers available in the standard SUMMiT-V™ process.

3.1 Serial-Link Machine Architecture

Serially stacked joint architecture is the most common choice to arrange joint axes for motion control equipment. A serial linkage machine consists of a number if independently controlled joints or axes where the first joint carries the second, which carries the third and so on until the number of independent joint axes reaches the desired number of motion degrees of freedom. This architecture is most commonly used in industrial robots, machine tools and coordinate measuring machines (Figure 3-2).

(a) **(b)** **(c)**

Figure 3-2 – Examples of common machines that use serial-linkages (a) KUKA KR125 industrial robot, (b) Cincinnati VMC-1250C machine tool, and (c) a Zeiss Prismo coordinate measuring machine.

Macro scale design and control of such systems is a mature technology that may be leveraged. However there are difficulties in shrinking this type of architecture down to the microscale, especially in light of the constraints in Table 3-1. Table 3-2 shows how a serial linkage type machine would stack-up against the design criteria in Table 3-1.

Table 3-2 – Serial mechanisms versus design constraints.

Constraint	Reason
All constituent parts must be 2D and planar.	Potentially very well.
All constituent parts must be fully assembled and interconnected during the fabrication process.	Doubtful. There will undoubtedly be some sort of manual or semi-automatic assembly step. At the very least components will be hinged and then erected and connected together to form out of plane guideways and joint axes .
Constituent parts must be able to be connected to one another in an arbitrary order.	Doubtful. As in the case of macro serial machine, each part will more than likely need to be individually designed and engineered. The designer only has four levels of structural poly silicon available which more than likely will not be enough for all of the different stacked components. Also the addition of rotary degrees of freedom may be extremely difficult.
A large number of device designs must be enabled from a small finite number of parts or building blocks.	Doubtful. As in the case of macro serial machine, each part will more than likely need to be individually designed and engineered.
Stacked actuators must be avoided to prevent cross talk between axis command signals.	At least very difficult. Due to the nature of the SUMMiT-V™ process stacked actuators are not possible. If it were possible it would require pigtailed signal lines that are prone to electrostatic attraction to grounded surfaces and fatigue from mechanical cycling.

Despite these problems there are some researchers that have built serial spatial devices in silicon (Figure 3-3).

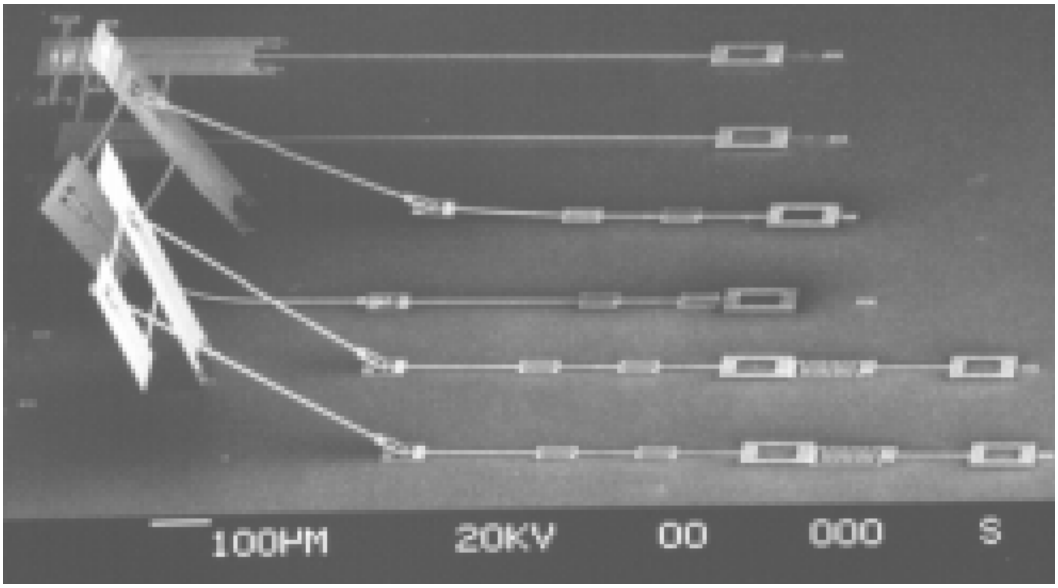

Figure 3-3 – Out of plane Serial linkage device in silicon MEMS [29].

3.2 Parallel-Link Machine Architecture

Parallel mechanisms differ from serial mechanisms in that they do not have a single structural loop that connects the mechanism coordinate frame to the end effector's frame (revisit Figure 3-1). Notice that each actuator is connected to both the ground and end effector coordinate frames.

A great deal of work was done in the 1990's to adapt the parallel actuator arrangement for use in machine tools and robots [look in 30-31 a many good sources of information]. Two main types of these machines evolved 1990's.The first type uses fixed-location joints with interconnecting actuated extensible links connecting the platform joints to the base joints (Figure 3-6). The second type of parallel machine architecture utilizes moveable joints with fixed-length struts (Figure 3-7).

(a) **(b)** **(c)**

Figure 3-6 – Different parallel link machine tools (a) Ingersoll Milling Octahedral Hexapod, (b) Giddings and Lewis Variax, and (c) Okuma Cosmo Center.

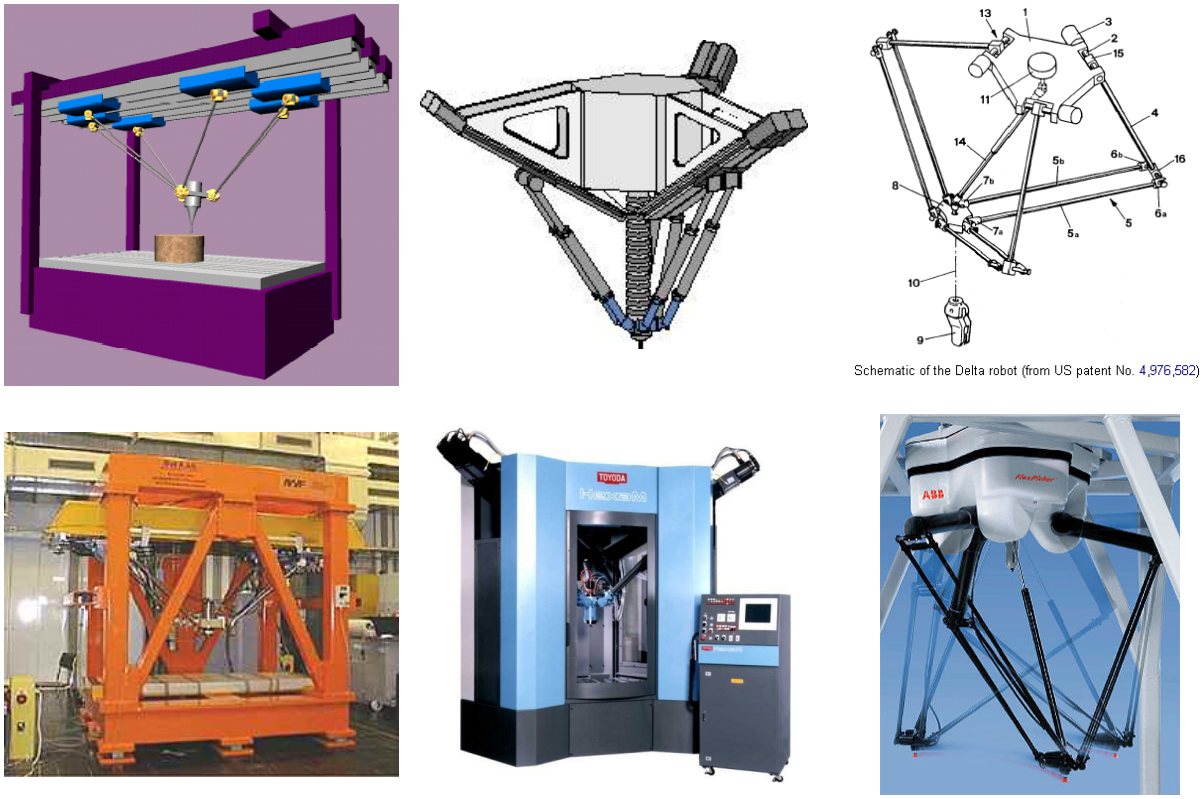

(a) **(b)** **(c)**

Figure 3-7 – Variable joint spatial location and fixed-length strut parallel mechanism machine tools (a) The Hexaglide from Switzerland, (b) the Toyoda Hexam and (c) the ABB IRB340 FlexPicker robot.

What is immediately advantageous about these parallel link mechanisms in light of the compatibility of the serial mechanisms with surface micromachining methods is the absence of stacked guideways and actuators (revist Tables 3-1 and 3-2). However there is a distinct difference in operation of the actuators between the two types of PKMs. The first type requires the drive struts to either telescope or to translate through the drive motors. One would have a great deal of difficulty creating telescoping drive links in planar MEMS processes that could also move spatially. However the second type is more promising. The drive motors may be located on a plane. With the drive motors and telescoping actuators in a plane, fixed length struts may be used to connect the actuators to the motion platform. Table 3-3 summaries how the fixed length strut PKM matches the design and process criteria.

Table 3-3 – Fixed length strut PKM versus design constraints.

Constraint	Reason
All constituent parts must be 2D and planar.	Potentially very well.
All constituent parts must be fully assembled and interconnected during the fabrication process.	Potentially very well. The devices pictured in Figure 3-7 all can be modified to fit in a planar configuration. The struts and platform would however be in a singular configuration.
Constituent parts must be able to be connected to one another in an arbitrary order.	A toolbox of parts in the micro domain can be perfected that emulates what INA has done for machine tools and robots.
A large number of device designs must be enabled from a small finite number of parts or building blocks.	From Figure 3-6 and 3-7 it is obvious that a discrete set of parts enables many configurations. With a general toolbox of such parts a number of different mechanisms may be assembled.
Stacked actuators must be avoided to prevent cross talk between axis command signals.	From Figure 3-7 each drive link has its own non-stacked guideway. This can be replicated in the micro domain as well.

So just from a logical look at the basic types of serial and parallel linkage it becomes apparent that a PKM design with fixed location actuators and fixed length drive struts has the fewest obvious drawbacks in light of design and fabrication criteria. The next step is to determine what are the necessary building blocks for such mechanisms.

Again one can borrow from the large body of knowledge in PKM machine tools and robotics. In the beginning of the PKM machine tool movement, every component had to specially made and manufactured. The Swiss company INA soon offered whole families of special joints, connectors and actuators that could be pieced together arbitrarily to build whole machines. This is the type of modular toolbox of parts that a MEMS designer would need as well to have the flexibility to build virtually any type of PKM mechanism.

3.3 Options for Parallel Linkages

3.3.1 Planar Motion

Planar motion refers to motion constrained to only move in a plane. The device can move left and right, forward and backward and rotate in the plane. However it is not able to move up or down out of the plane.

Even with these constraints a number of very interesting and useful permutations of planar mechanisms are possible using rotary and/or linear joints. A few are shown in Figure 3-8. The numbers grow when different types of actuation and special geometries are applied

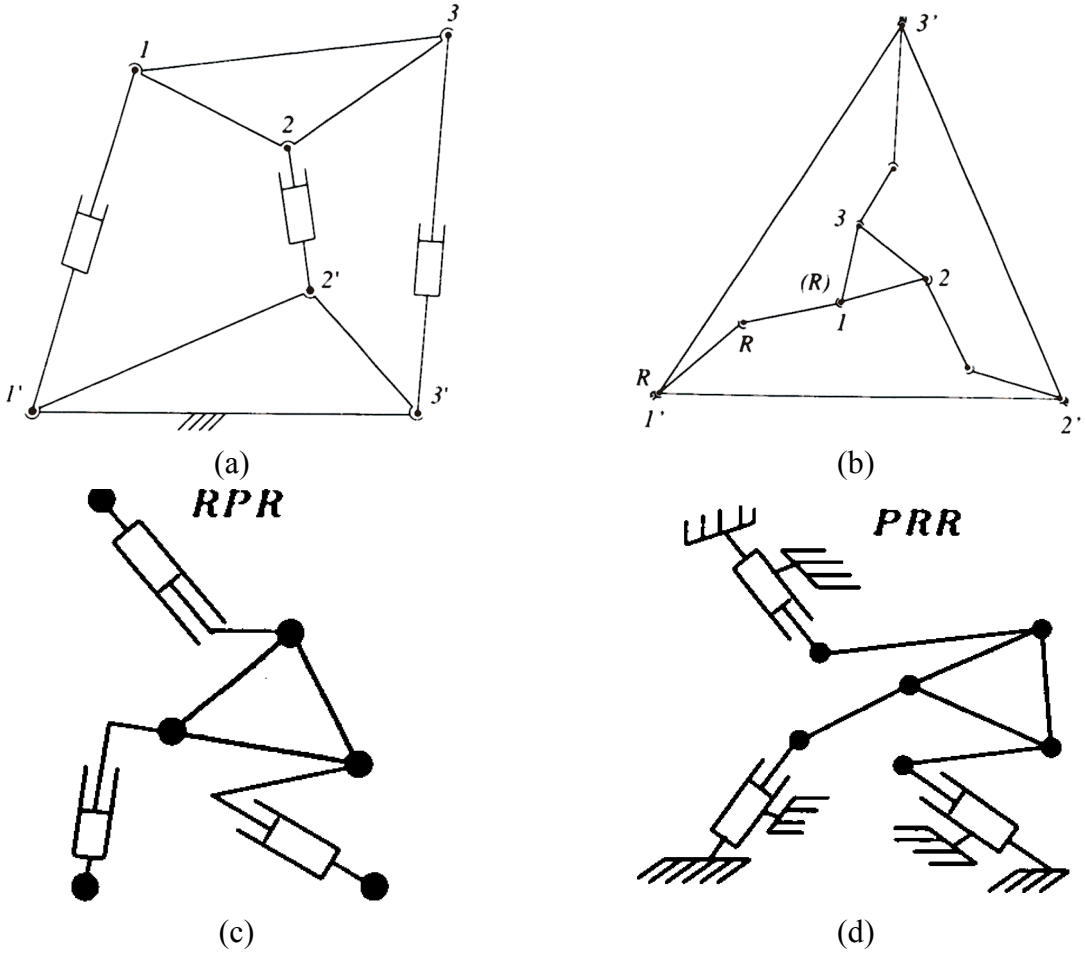

Figure 3-8 – Schematics of different types of planar PKM mechanisms (a) and (b) [30], (c) and (d) [31].

3.3.2 Spatial Motion

The options for the different types of PKM mechanism producing different types of motion greatly increase if one thinks about mechanisms that perform spatial motion (Figure 3-9).

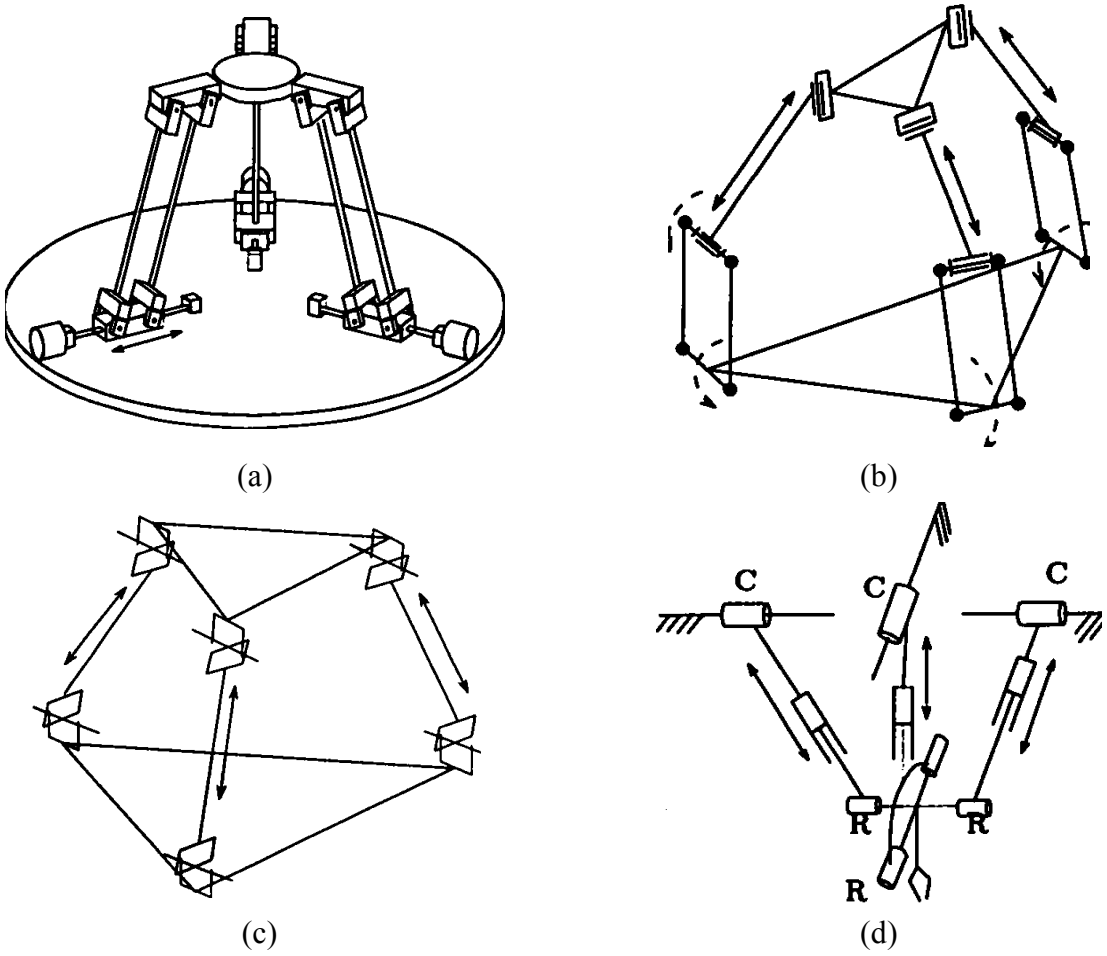

Figure 3-9 – Different types of spatial PKM mechanisms (a) , (b), (c) and (d) [31].

How does one figure out though how many links and joints, which type of joints should/can be used and how many controllable degrees of freedom result at the end effects or manipulator? For the most part this can be summarized in a single table (Table 3-4).

Table 3-4 – Relation of platform degrees of freedom to number and distribution of joint degrees of freedom.

Degrees of Freedom (DOF)	Number of Independent Kinematic Loops	Sum of All Joint DOF	Connectivity
2	1	8	4,4 5,3 6,2
3	***2***	***15***	***5,5,5*** 6,5,4 6,6,3
4	3	22	6,6,5,5 6,6,6,4
5	4	29	6,6,6,6,5
6	5	36	6,6,6,6,6,6

Table 3-4 is used by first determining how many desired controllable degrees of freedom are desired at the platform. This dictates the number of independent kinematic loops that are present in the mechanism. This also dictates the number of all degrees of freedom in the joints that are present. Connectivity then depends on how the designer would like to distribute the joint degrees of freedom along the kinematic loops.

For instance, say one wants a device with three degrees of freedom. A 3-DOF device has two independent loops and requires three motion inputs. Let's say that each motion input is a separate kinematic chain or leg that constrains the platform to the base frame. If the device were symmetrical each leg would have five degrees of freedom associated with (however as Table 3-4 shows there are other distributions of the degrees of freedom). Now the designer knows that he/she must create a kinematic chain that has five degrees of freedom in it. One of these is controlled as the motion input to the system. The other four degrees of freedom have to be passive and must be reolved in two joints (one at the platform, one at the base). This leads to the joint freedom pairs of 1 and 3 (a hinge and a ball joint) or 2 and 2 (two different types of Hooke joints). So this means that the designer must at least have at his/her disposal joints with one, two and three degrees of freedom.

3.4 Joint Design for Correct Constraint

From the discussion in section 3.3 it is clear that many different types of PKMs are made feasible by a finite number of joints with one, two and three DOF. The following sections detail the types of joints available utilizing only revolute DOF.

3.4.1 One Degree of Freedom (DOF)

There are two basic types of one-DOF joints – pin joints and hinge joints with fundamentally different motions with respect to the fabrication plane.

Incorporated in the SUMMiT-V process is a special construction called a "pin joint cut" which allows the designer to simply create a pin joint of any size anywhere he/she wishes. These pin joints allow motion in the fabrication plane about an axis normal to the plane (or about the z-axis direction vector) (Figure 3-10a).

Hinge joints on the other hand allow motion about an axis in the fabrication plane. Hinge joints can be made by appropriately patterning and layering Poly1-3 (Figure 3-10b).

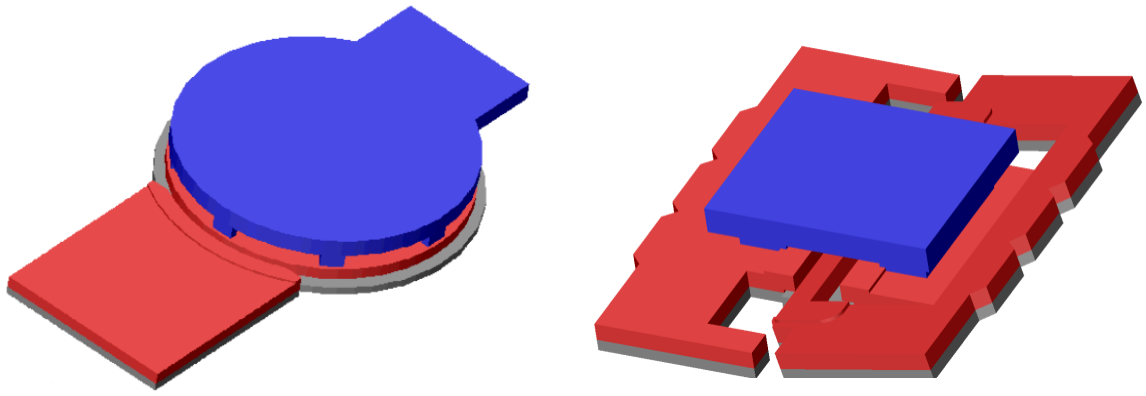

(a) **(b)**

Figure 3-10 – One-DOF joints: (a) pin joints and (b) hinge joints.

3.4.2 Two DOF Joints

Joints the have two DOF are extremely important in engineering and enable many different types and constructions of mechanisms. Of particular importance are the universal or "Hooke" joints that have two intersecting, mutually perpendicular joint axes. In the MEMS planar fabrication world these two-DOF joints have four fundamentally different constructions. Depending on the type of motion desired and/or design constraints the designer will either require or prefer a certain type of construction to another (Figure 3-11).

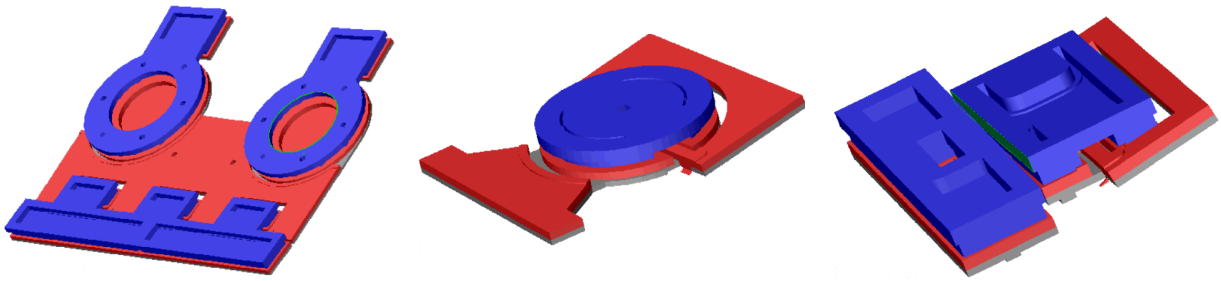

(a) **(b)** **(c)**

Figure 3-11 – Two-DOF joints with orthogonal joint axes: (a) nonintersecting pin and hinge, (b) intersecting pin and hinge and (c) two intersecting hinges.

3.4.3 Three DOF Joints

A three-DOF joint that approximated a spherical joint may be constructed from two, two-DOF joints. This joint uses one first-construction joint and one second construction joint to create a joint with three mutually perpendicular and intersecting DOF (Figure 3-12).

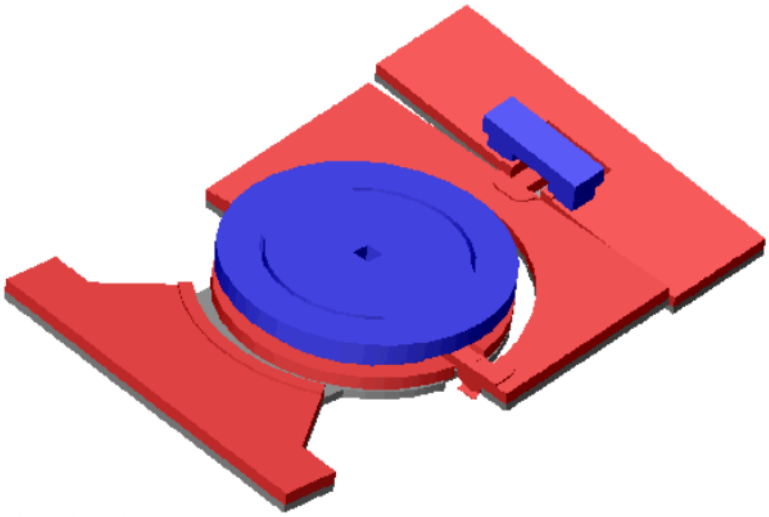

Figure 3-12 – Three-DOF joint emulating a spherical joint in MEMS.

3.4.4 Spatial Four-Bar Linkages

Four type-II two-DOF joints may be put together to create a spatial four-bar where links 1 and 4 are of equal length and 2 and three are of equal length forming a collapsible parallelogram connected by pin joints. The hinge joints at either end allow the collapsible parallelogram to flex out of the fabrication plane (Figure 3-13).

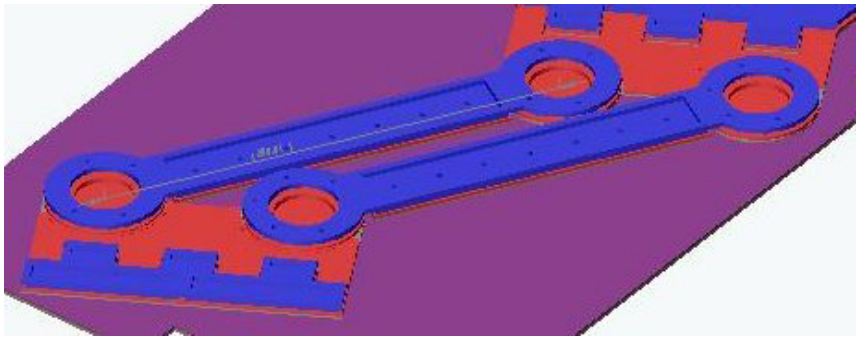

Figure 3-13 – A spatial four-bar linkage in MEMS.

4. MEMS Linear Stepping Track Drives (LSTD)

A requirement at the outset of the project was to develop platforms that are motion controllable. This means that the control system must read and interpret commands from a path plan command file (M/G code) and then apply the appropriate drive signals voltages in time correctly to the actuators. The control systems will be addressed in forth coming sections. This section will deal specifically with motion controllable MEMS linear actuators.

In general there are two kinds of motion control systems – closed loop and open loop. In a closed loop system the motor current loop is closed around the position error. The position error is the difference between the commanded position and the measured amount of motion from the position sensor(s). It is a requirement of a closed loop system to measure the current position of the drive axes in-situ by some means (linear scale, laser, resolver, encoder, etc.).

An open loop system differs from the closed loop system in that there is no position sensor, therefore no position error can be computed and used in the control loop to drive motor currents. In this case the actuation system must have some built-in passive means of controlling position. A common open loop position control system is the stepper motor.

A stepper motor typically has a series of independently addressable windings which when fired in the appropriate combination and order move the rotor or linear stage in one direction or the other. Every time a winding (or combination of windings) is energized the rotor or linear translation stage will move by a known, well-defined amount. By cycling through the winding firing order, net motion of the axis results. By keeping track of the number of steps and the order in which they occurred the position of the axis can be calculated. However if the motor is not appropriately sized (underpowered) or the mechanical axis system binds, the windings may fire without producing net motion of the axis.

Closed loop servo systems are commonplace in all meso- and macro-scale positioning systems. However at the micro scale the problem of creating a reliable and highly minaturized on-chip encoder or other type position transducer has not been solved. Without some kind of position transducer a closed loop system is not possible. However an open loop system is.

4.1. Theory of Operation

The linear stepping track drive (LSTD) operates on an age-old positive drive camming principle. An LSTD has a toothed rack that is moved by a series of linearly actuated drive teeth with matching tooth profiles as those on the track. As a set of drive teeth are actuated and come in contact with rack teeth, force is transferred from the drive teeth into the rack. When sufficient force has been applied from the drive teeth to the rack teeth, the rack moves. The drive teeth continue to engage the rack until the drive teeth reach the end of their stroke at which time the second set of drive teeth begin their rack engagement cycle. While the second set of drive are engaging the rack the first set retracts and clear the rack teeth. This cycle continues until the number of independently controlled drive teeth actuators has been exhausted, at which time the cycle starts over with the first drive teeth actuator (Figure 4-1).

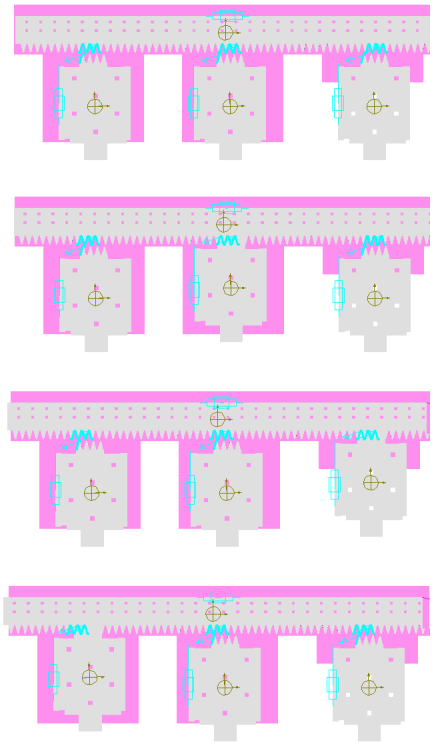

Figure 4-1 – Rack translation by camming action from cyclic drive teeth engagement.

4.2. LSTD Drive Resolution

Three factors affect LSTD single step resolution (r): (1) tooth pitch (λ), (2) number of layers of uniformly spaced teeth (n_L), and (3) the number of independently controlled drive teeth actuators (n_D) (Equation 4-1).

$$r = \frac{\lambda}{n_L n_D} \qquad 4\text{-}1$$

Equation 4-1 is deceptively simple but actually spurs many different non-intuitive possibilities when considering actuator resolution.

EXAMPLE:

A linear actuator is needed that has a 250nm (0.25μm) single step resolution. How many independently controlled actuators are needed if it is to be built using SUMMiT-V?

Assume a 6μm tooth pitch:

$$r = \frac{6\mu m}{24} = 0.25\mu m$$

From Equation 4-1 $(n_L)(n_D)=24$. SUMMiT-V has a maximum of four structural layers of polysilicon, which yields the following possibilities:

n_L	n_D
1	24
2	12
3	8
4	6

This means that one can build a 1, 2, 3 or 4 level device that requires 24, 12, 8 or 6 independently controlled actuators respectively. Since it is desirable to have as few drive signals as possible a 4-level, 6-actuator device is tempting. However it is better possibility that you could build one in three layers requiring eight independent drive signals given the complexities of dealing with layers Poly1 and Poly2.

4.3. Minimum Tooth Spacing for Smooth Stepping

Looking back at Equation 4-1 it is tempting to think that one could build a rack with smaller and smaller tooth spacing to get a smaller and smaller least count motion. In SUMMiT-V at least there is a limit as to how small the tooth spacing can be and still achieve cog-free motion. In the overview of the SUMMiT-V process it was stated that SUMMiT-V has diffraction limited resolution of 1μm (using the lithography machines and processes currently available in the MDL). Solid features smaller than 1μm will not form and conversely gaps less than 1μm will be filled in completely. This 1μm feature resolution limits the sharpness of the points of the drive teeth to a radius of 0.5μm (Figure 4-2). It is this radius that causes cogging problems between the drive and rack teeth.

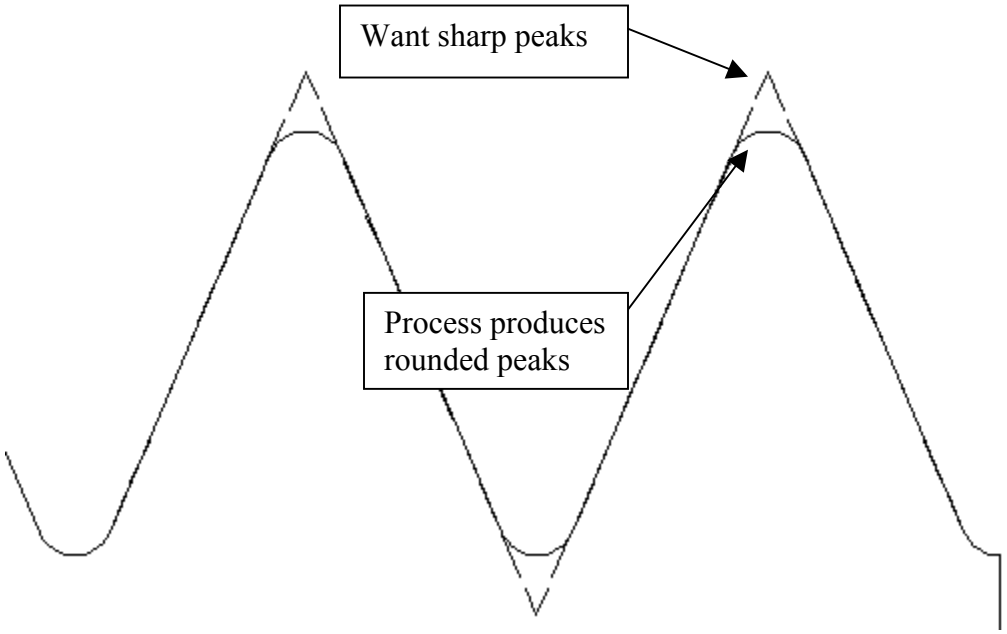

Figure 4-2 – Effect of diffraction limited lithography resolution of 1μm on the sharpness of rack drive teeth.

One could imagine two drive teeth trying to mesh. If they impact radius to radius the resultant force vector would have a large component not favorable to rack motion. Therefore it is more desirable to have the teeth impact on the flanks and avoid radius-to-radius contact all together (Figure 4-3). What would be preferable would to be able to intelligently select drive parameters that would guarantee flank-to-flank contact during a normal stepping sequence.

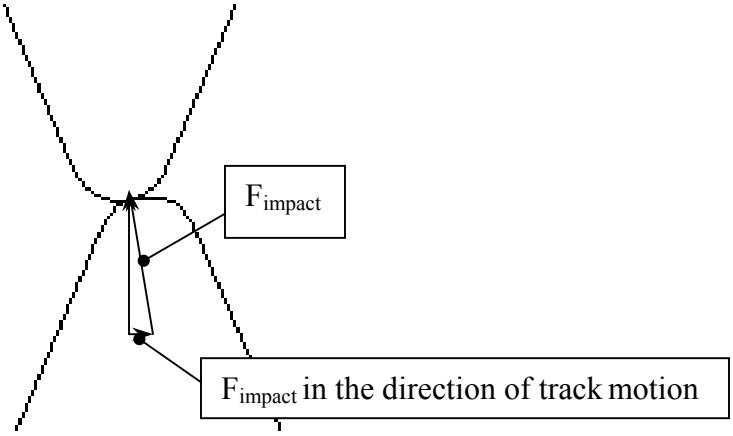

Figure 4-3 – Radius-to-radius contact produces large contact forces unfavorable to rack motion.

Consider a point on the rack (A) where the radius is tangent to the flank near the pinnacle of the tooth, and a point (B) at the corresponding location near the root of the tooth Figure 4-4).

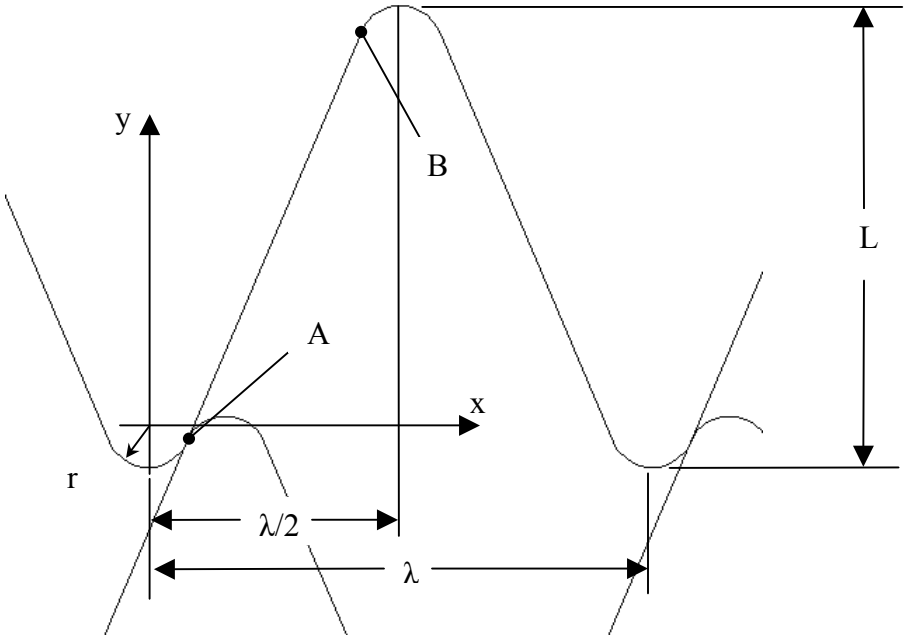

Figure 4-4 – Location of points A and B on a pair of drive and rack teeth.

From these two points one can develop the equations for the condition of the maximum distance between the drive tooth and rack valley centerlines while guaranteeing flank-to-flank tooth engagement (Equation 4-2).

$$\begin{aligned}\overline{A} &= \left(r\cos(\theta)\right)\hat{i} - \left(r\sin(\theta)\right)\hat{j} \\ \overline{B} &= \left(\frac{1}{2}\lambda - r\cos(\theta)\right)\hat{i} + \left(L - 2r + r\sin(\theta)\right)\hat{j} \\ AB &= \overline{B} - \overline{A}\end{aligned} \qquad 4\text{-}2$$

$$\overline{A}\cdot AB = \frac{1}{2}r\left(\lambda\cos(\theta) - 4r - 2L\sin(\theta) + 4r\sin(\theta)\right) = 0$$

Solving for the positive solution for theta satisfies the condition in Equation 4-2. The largest distance between the drive tooth center and the rack tooth valley without radius-to-radius contact is then calculated (Equation 4-3).

$$\text{Maximum Smooth Step Distance} = \frac{\lambda}{2} - 2r\cos\theta \qquad 4\text{-}3$$

The condition for smooth stepping resolution is given in Equation 4-4.

$$\lambda\left(\frac{n_L - 1}{2n_L} + \frac{1}{n_L n_D}\right) \le \frac{\lambda}{2} - 2r\cos\alpha \qquad 4\text{-}4$$

Using Equations 4-1 to 4-4, one can build table for various track parameters (L and λ), number of evenly spaced track layers (n_L) and number of drives (n_D) in order to investigate various drive and parameter combinations that yield smoothly stepping track systems and their resolutions (Table 4-1).

Using Table 4-1 one can develop the specifications for the tooth profiles for a stepping track drive that produces smooth steps. The relation for the distance between the sets of drive teeth is given in Equation 4-5.

$$\text{Distance of drive tooth \#1 peak from track valley}: \quad d_1 = \frac{\lambda}{n_L n_D}$$

$$\text{Spacing of each subsequent drive tooth}: \qquad d_i = d_1 + \sum_{1=2}^{n_D} N_i - \lambda\left(\frac{n_D - 1}{n_L n_D}\right) \qquad 4\text{-}5$$

Table 4-1 - Feasible layer, number of drives and resolution combinations for smooth stepping.

L (μm)		6	6.5	7	7.5	8	8.5	9	9.5	10
λ (μm)		6	6.5	7	7.5	8	8.5	9	9.5	10
n_L	n_D	Drive Resolution (μm)								
1	**3**	**2.000**	**2.167**	**2.333**	**2.500**	**2.667**	**2.833**	**3.000**	**3.167**	**3.333**
2	**3**	1.000	1.083	1.167	1.250	1.333	1.417	1.500	1.583	1.667
3	**3**	0.667	0.722	0.778	0.833	0.889	0.944	1.000	1.056	1.111
1	**4**	**1.500**	**1.625**	**1.750**	**1.875**	**2.000**	**2.125**	**2.250**	**2.375**	**2.500**
2	**4**	0.750	0.813	0.875	**0.938**	**1.000**	**1.063**	**1.125**	**1.188**	**1.250**
3	**4**	0.500	0.542	0.583	0.625	0.667	0.708	0.750	0.792	0.833
1	**5**	**1.200**	**1.300**	**1.400**	**1.500**	**1.600**	**1.700**	**1.800**	**1.900**	**2.000**
2	**5**	0.600	**0.650**	**0.700**	**0.750**	**0.800**	**0.850**	**0.900**	**0.950**	**1.000**
3	**5**	0.400	0.433	0.467	0.500	0.533	0.567	0.600	**0.633**	**0.667**
1	**6**	**1.000**	**1.083**	**1.167**	**1.250**	**1.333**	**1.417**	**1.500**	**1.583**	**1.667**
2	**6**	**0.500**	**0.542**	**0.583**	**0.625**	**0.667**	**0.708**	**0.750**	**0.792**	**0.833**
3	**6**	0.333	0.361	0.389	0.417	0.444	**0.472**	**0.500**	**0.528**	**0.556**
1	**7**	**0.857**	**0.929**	**1.000**	**1.071**	**1.143**	**1.214**	**1.286**	**1.357**	**1.429**
2	**7**	**0.429**	**0.464**	**0.500**	**0.536**	**0.571**	**0.607**	**0.643**	**0.679**	**0.714**
3	**7**	0.286	0.310	0.333	0.357	**0.381**	**0.405**	**0.429**	**0.452**	**0.476**
1	**8**	**0.750**	**0.813**	**0.875**	**0.938**	**1.000**	**1.063**	**1.125**	**1.188**	**1.250**
2	**8**	**0.375**	**0.406**	**0.438**	**0.469**	**0.500**	**0.531**	**0.563**	**0.594**	**0.625**
3	**8**	0.250	0.271	0.292	**0.313**	**0.333**	**0.354**	**0.375**	**0.396**	**0.417**
1	**9**	**0.667**	**0.722**	**0.778**	**0.833**	**0.889**	**0.944**	**1.000**	**1.056**	**1.111**
2	**9**	**0.333**	**0.361**	**0.389**	**0.417**	**0.444**	**0.472**	**0.500**	**0.528**	**0.556**
3	**9**	0.222	0.241	0.259	**0.278**	**0.296**	**0.315**	**0.333**	**0.352**	**0.370**
1	**10**	**0.600**	**0.650**	**0.700**	**0.750**	**0.800**	**0.850**	**0.900**	**0.950**	**1.000**
2	**10**	**0.300**	**0.325**	**0.350**	**0.375**	**0.400**	**0.425**	**0.450**	**0.475**	**0.500**
3	**10**	0.200	0.217	**0.233**	**0.250**	**0.267**	**0.283**	**0.300**	**0.317**	**0.333**
1	**11**	**0.545**	**0.591**	**0.636**	**0.682**	**0.727**	**0.773**	**0.818**	**0.864**	**0.909**
2	**11**	**0.273**	**0.295**	**0.318**	**0.341**	**0.364**	**0.386**	**0.409**	**0.432**	**0.455**
3	**11**	0.182	0.197	**0.212**	**0.227**	**0.242**	**0.258**	**0.273**	**0.288**	**0.303**

bold Feasible combinations.
shaded Infeasible combinations.

4.4. Calculation of LSTD Force Output

It is conceivable that LSTDs could be actuated by a number of different means. The means by which LSTDs are actuated it not as important as the multiplication of the input force generated by the LSTD. LSDTs not only provide a means to control position by counting steps, they also act as a force multiplier. A simple quasi-static force balance analysis including the effects of friction gives a range of values for mechanical advantage of an LSTD for different combinations of tooth angle and coefficient or static friction (Figure 4-5).

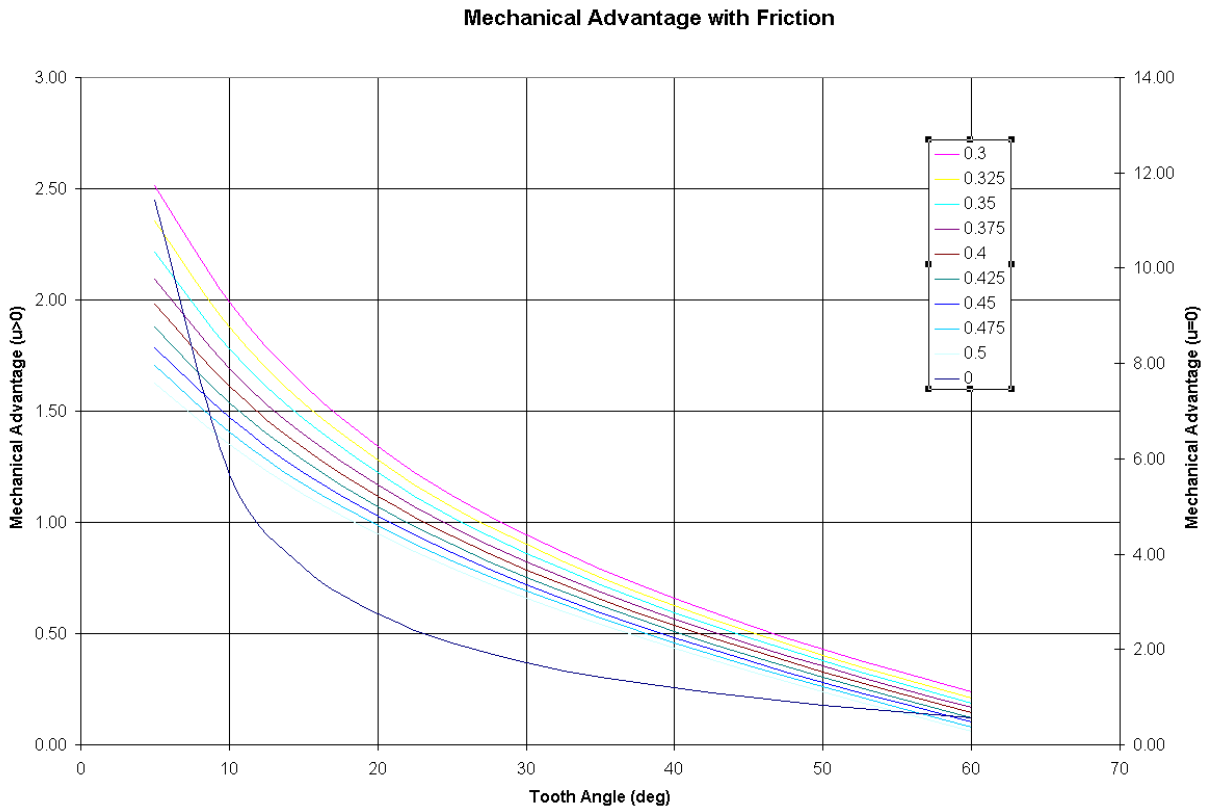

Figure 4-5 – Relation between tooth angle, static friction and mechanical advantage.

EXAMPLE:

What is the range of mechanical advantage to be expected from a LSTD with the following configuration?

n_L (μm)	2
n_D (μm)	5
L (μm)	7
λ (μm)	7

Using Equations 4-1 to 4-4 the resolution of the LSTD is 0.7μm and the tooth half-angle (θ) is 22°. Using Figure 4-5 a range of 1.25-0.9 of mechanical advantage for a static friction range of 0.3-0.5 is to be expected.

4.5. Generation 1 – Double-Sided Drive Tape

This first generation of LSTD was a double-sided tape drive (Figure 4-7). It consisted of a single track made from three laminated layers polysilicon 6.5μm thick and 25μm wide. It had teeth on either side with a 4.75μm tooth pitch. The track was driven by three Sandia high performance comb drives (HPCDs) yielding a resolution of 1.58μm per step.

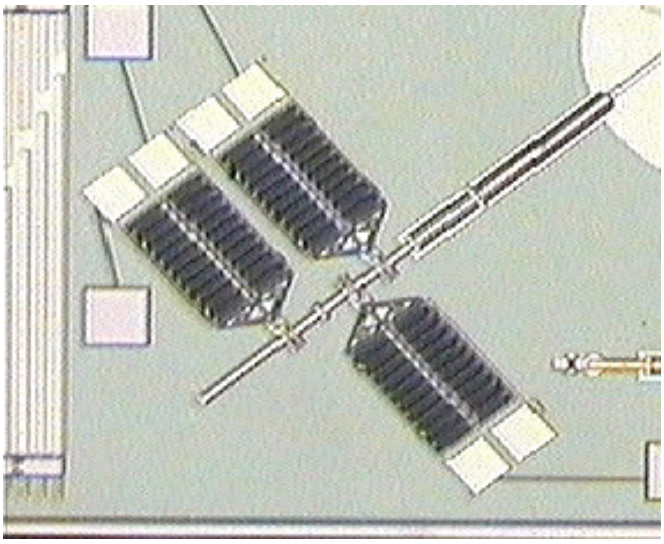

Figure 4-6 – Generation #1 double sided tape LSTD.

This LSTD did not perform well in testing. During operation the track had a tendency to bend and bind against the linear guides, which would either stop the track completely or cause sporadic motion when the teeth would suddenly slip in the guides and launch the track unpredictably. However the track did demonstrate that the concept of an LSTD in MEMS was possible.

These devices were tested in the LIGHT Lab in building 858. Signals were applied to these drives by three signal generators running in conjunction with the Sandia developed MicroDriverII software.

4.6. Generation 2 – Single-Sided High Stiffness

The second generation of the LSTD was a three-actuator, single-sided design with rack teeth actuators only on one side (Figure 4-7) that also had a 1.58μm resolution. The track was made from a lamination of Poly1 and Poly2 while the teeth were a lamination of Poly1-3.

To circumvent the problem of track binding from flexing during actuation, the track was supported its entire length on one side. A top cover of Poly3 had a dimple cut that ran the length of the cover that fit into an alignment groove in the top of the track which was formed by a gap in the Poly2 layer of the track. The alignment groove provided transverse constraint while allowing straight longitudinal motion of the track (Figure 4-8).

This design was successfully actuated and tested up to actuator drive frequencies of 1KHz. Tests also showed that repeatable high-speed motions were possible using the LSTD (10's of mm/sec).

This design did have two problems. The first was a design error. A set of tabs prevented the actuator linear guides from working properly (Figure 4-9). These tabs resulted from stray marks left on the AutoCAD design mask that for some reason were not deleted before the design was submitted for fabrication. During testing these tabs could be broken off using the tip of a probe. This design flaw was easily remedied in future versions of the LSTD.

Figure 4-7 – Generation #2 single-sided LSTD.

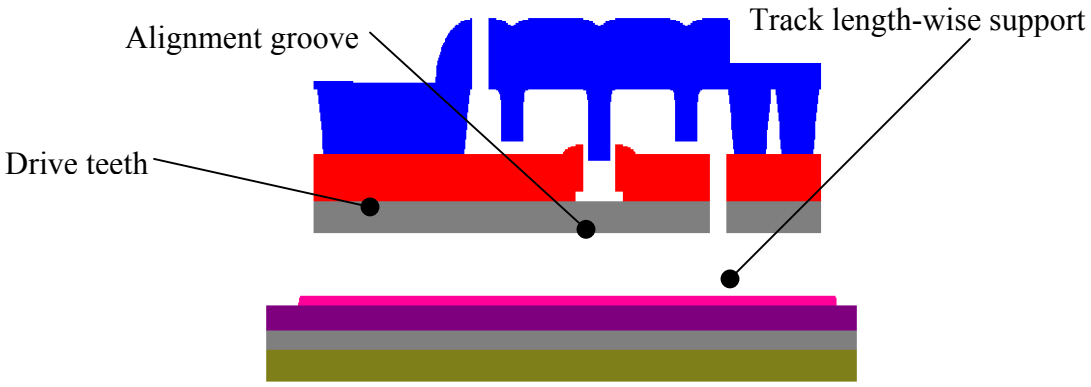

Figure 4-8 – Cross sectional view of Generation #2 single-sided LSTD.

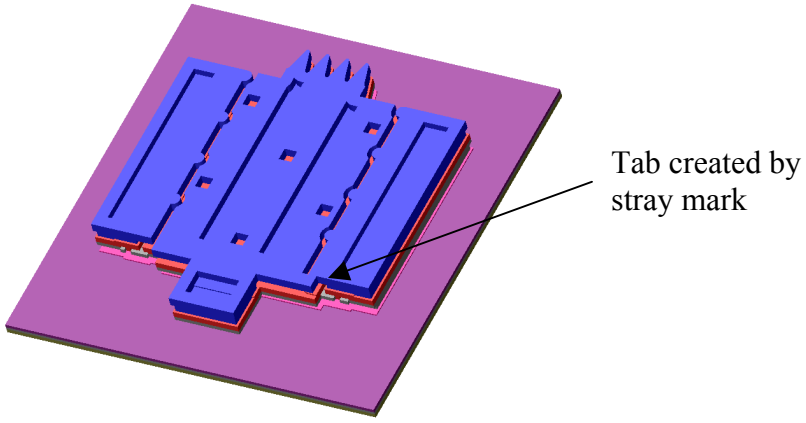

Figure 4-9 –Solid model showing tabs created by stray marks that locked-up the Generation #2 HPCD actuators.

The second was the problem of cogging due to the radius-to-radius impact of the drive teeth on the rack teeth. This problem prompted the development of the design rules that were previously mentioned in Equations 4-1 to 4-5.

4.7. Generation 3 – Single-Sided High Stiffness

The third generation of the LSTD was immensely successful. The single-sided track design that appeared in generation #2 was reused with some cosmetic changes, while the stepping scheme benefited from the smooth step analysis prompted by the cogging problems in generation #2.

The single-sided version of Generation #3 had a tooth pitch of 6 microns, a tooth length of 5.5 microns and could achieve 2 microns per step of repeatable motion using three HPCD actuators. Three versions of the third generation single-sided LSTD were built – low, medium and high force versions. These versions differed from each other only in the force output of the HPCDs used (Figure 4-10). The low force HPCDs used three double banks of electrostatic comb fingers. The medium used four, while the high used five. It was estimated that the different HPCD versions could put out 60, 80 and 110uN of force respectively.

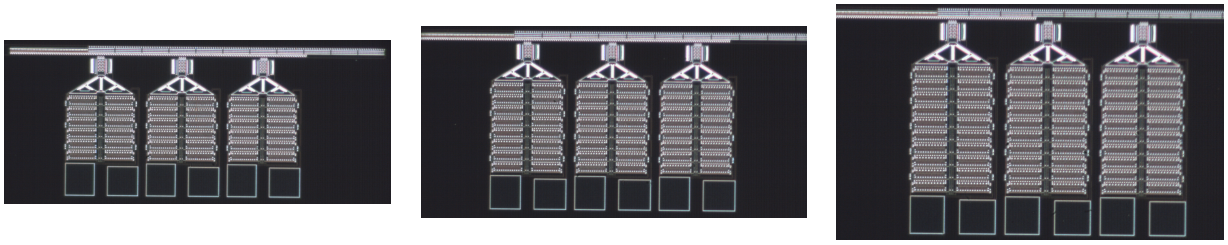

(a) **(b)** **(c)**

Figure 4-10 – Generation #3 signle-sided LSTDs (a) low force (SSL), (b) medium force (SSM) and (c) high force (SSH).

During testing these drive exhibited high-speed motion with very high positional epeatability of the rack. Rack speeds of up to 100mm/s were attained. Table 4-2 summarizes the test results for the single-sided LSTDs.

Table 4-2 Results for Generation #3 single-sided LSTDs.

Drive Design	Voltage Level	Speed (mm/sec)		
		20	40	100
SSL	40	P	P	F
	60	F	P	F
	80	F	F	F
SSM	40	P	P	F
	60	P	P	M
	80	F	F	P
SSH	40	P	M	F
	60	P	P	M
	80	F	F	M

P - Pass, perfect repeatability and displacement over all tests.
M - Marginal, nearly full displacement, not repeatable motion.
F - Fail, no or very little net motion of track.

4.8. Generation 3 – Double-Sided High Stiffness

The double-sided version of the third generation LSTDs had a completely different rack design than that of the first generation LSTD (Figure 4-11) in that the rack was completely constrained from underneath by a Poly1-2 linear guideway that constrains the track laterally along its entire length instead of at discrete locations (Figure 4-12). The tooth pitch, number of drives and resolution were the same as its single-sided version. Test results of the Generation #3 double-sided version of the LSTD show that the double-sided versions were not as flawless or well behaved as those of the single-sided LSTD's.

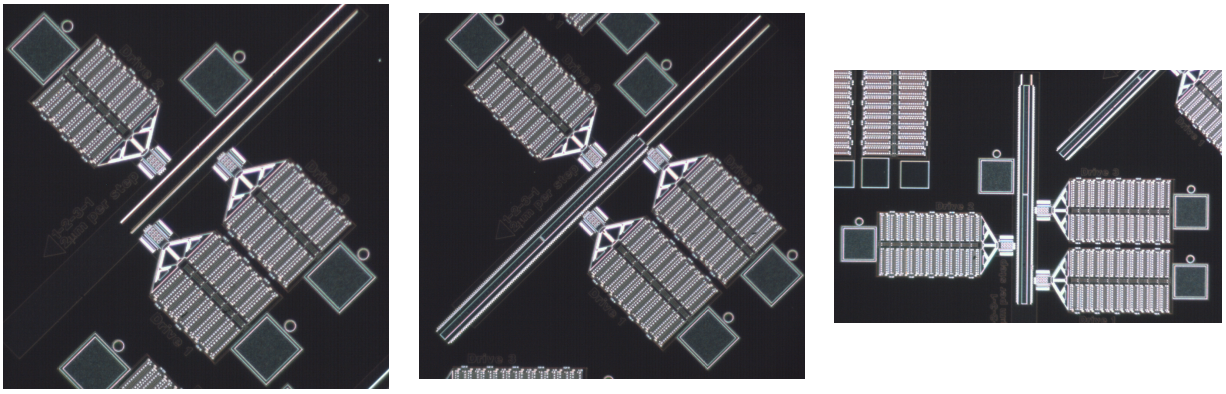

(a) (b) (c)

Figure 4-11 Generation #3 double-sided LSTDs (a) low force (DSL), (b) medium force (DSM) and (c) high force (DSH). cross sectional view of track showing Poly1-2 linear guideway.

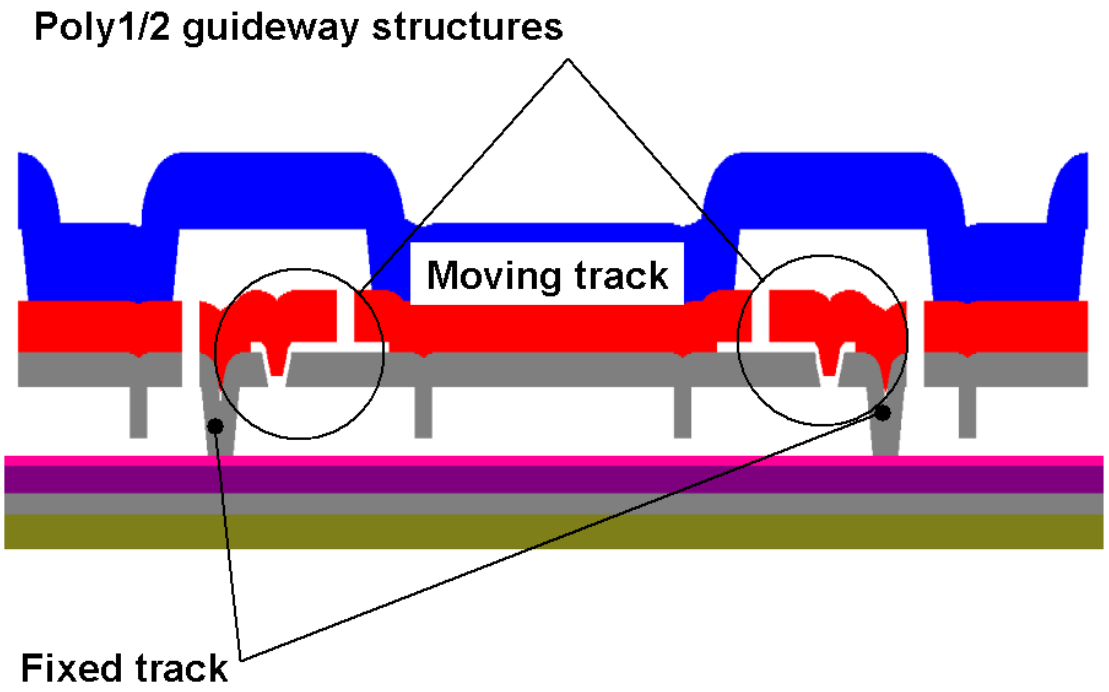

Figure 4-12 Generation #3 double-sided LSTD cross sectional view of track showing Poly1-2 linear guideway.

Cogging was much more evident in the double-sided versions and low speed performance was prone to step skipping which caused the linear motion of the drives to not be repeatable (Table 4-3). It is believed that this is due to the fact that the drives are not constantly loaded against one side of the track as in the single-sided LSTD's. In the single-sided versions the track is forces against the guideway by the force of all three HPCD actuators. However the double-sided versions are forced back and forth laterally as the opposing HPCD actuators fire. The very small compliance (0.2 microns) between the track and the guideway is enough to allow the track to angularly displace as it is moved down the track. The result is that the set of drive teeth corresponding to the next HPCD to fire are not properly aligned with the track teeth causing the device to cog or stall for an instant. However at higher speeds the double-sided LSDT's appeared to perform very well in that they consistently repeated linear motions (Table 4-3).

Table 4-3 Results for Generation #3 double-sided LSTDs.

Drive Design	Voltage Level	Speed (mm/sec)		
		20	40	100
DSL	40	I	I	I
	60	I	I	I
	80	I	I	I
DSM	40	M	M	F
	60	P	M	F
	80	P	P	F
DSH	40	P	M	M
	60	F	P	P
	80	F	M	M

P - Pass, perfect repeatability and displacement over all tests.
M - Marginal, nearly full displacement, not repeatable motion.
F - Fail, no or very little net motion of track.
I - Incomplete data tracks fell off during release process.

4.9. Generation 3 – Motion Control Algorithms

From previous testing experiences it was determined that the MicroDriver software was not adequate to address the problem of positional control of the track. The MicroDriver II software was primarily intended for the application of repetitive signals, not for handling more specialized acceleration and deceleration curves needed in positional control. Therefore a new interface based on MATLAB was created.

The MATLAB-based interface allows the user to easily control the maximum acceleration, maximum velocity and total displacement (Figure 4-13) of the track through a graphical user interface (Figure 4-14).

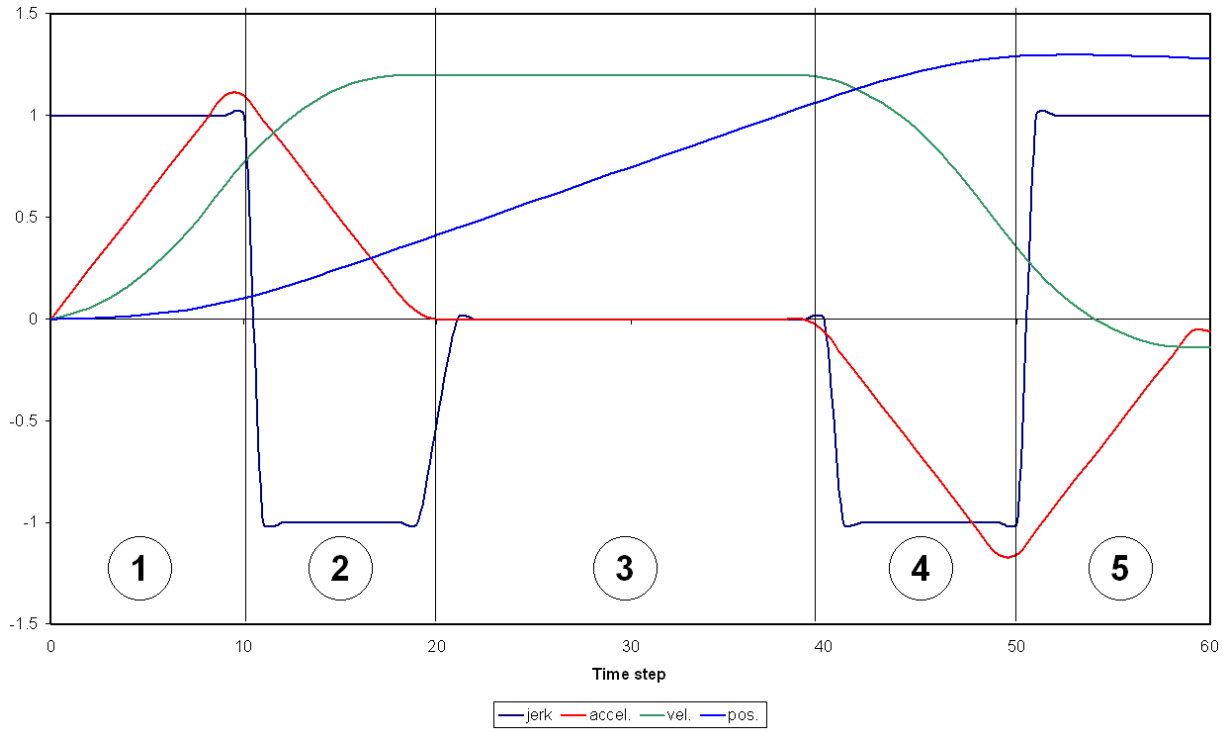

Figure 4-13 Time versus jerk, acceleration, velocity and position.

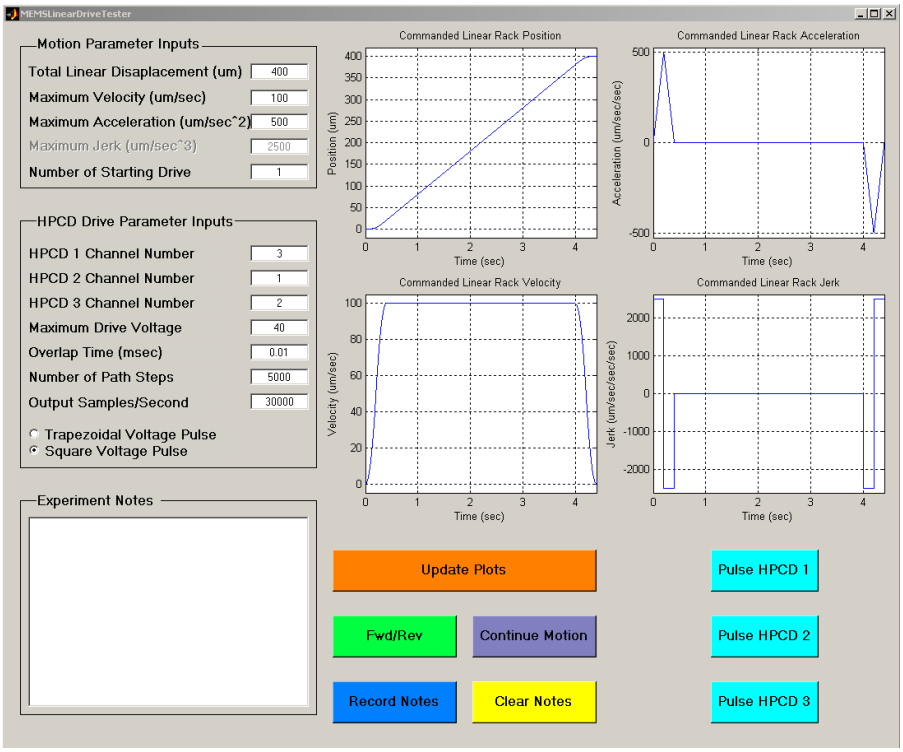

Figure 4-14 Graphical user interface for the LSTD control program.

Inputs from the interface are used to calculate the voltage-time record with respect to time (t) for each actuator using the Equations 4-6 through 4-9 (jerk, acceleration, velocity and position respectively) and the algorithm in Figure 4-15.

$$
\begin{aligned}
j_1 &:= \frac{Acom^{\,2}}{Vcom} \\
j_2 &:= -\frac{Acom^{\,2}}{Vcom} \\
j_3 &:= 0 \\
j_4 &:= -\frac{Acom^{\,2}}{Vcom} \\
j_5 &:= \frac{Acom^{\,2}}{Vcom}
\end{aligned}
\qquad 4\text{-}6
$$

$$
\begin{aligned}
a_1 &:= \frac{Acom^{\,2}\ t}{Vcom} \\
a_2 &:= -\frac{Acom\ (t\ Acom - 2\ Vcom)}{Vcom} \\
a_3 &:= 0 \\
a_4 &:= -\frac{Acom\ (t\ Acom - 2\ Vcom - \mathrm{D2}\ Acom)}{Vcom} \\
a_5 &:= \frac{Acom\ (t\ Acom - 4\ Vcom - \mathrm{D2}\ Acom)}{Vcom}
\end{aligned}
\qquad 4\text{-}7
$$

where:

$$
\mathrm{D2} := \frac{-2\ Vcom^{\,2} + Pcom\ Acom}{Vcom\ Acom}
$$

$$v_1 := \frac{Acom^2\, t^2}{2\, Vcom}$$

$$v_2 := -\frac{t^2\, Acom^2 - 4\, t\, Acom\ Vcom + 2\, Vcom^2}{2\, Vcom}$$

$$v_3 := Vcom$$

4-8

$$v_4 := -(t^2\, Acom^2 - 4\, t\, Acom\ Vcom - 2\, t\, Acom^2\, D2 + 2\, Vcom^2 + 4\, Vcom\ D2\ Acom + D2^2\, Acom^2)/(2\, Vcom)$$

$$v_5 := (t^2\, Acom^2 - 8\, t\, Acom\ Vcom - 2\, t\, Acom^2\, D2 + 16\, Vcom^2 + 8\, Vcom\ D2\ Acom + D2^2\, Acom^2)/(2\, Vcom)$$

$$p_1 := \frac{Acom^2\, t^3}{6\, Vcom}$$

$$p_2 := -\frac{t^3\, Acom^3 - 6\, t^2\, Acom^2\, Vcom + 6\, t\, Acom\ Vcom^2 - 2\, Vcom^3}{6\, Acom\ Vcom}$$

$$p_3 := \frac{(t\, Acom - Vcom)\, Vcom}{Acom}$$

4-9

$$p_4 := -(t^3\, Acom^3 - 6\, t^2\, Acom^2\, Vcom - 3\, t^2\, Acom^3\, D2 + 6\, t\, Acom\ Vcom^2 + 12\, t\, Acom^2\, Vcom\ D2 + 3\, t\, Acom^3\, D2^2 - 2\, Vcom^3 - 12\, Vcom^2\, D2\ Acom - 6\, Vcom\ D2^2\, Acom^2 - D2^3\, Acom^3)/(6\, Acom\ Vcom)$$

$$p_5 := (t^3\, Acom^3 - 12\, t^2\, Acom^2\, Vcom - 3\, t^2\, Acom^3\, D2 + 48\, t\, Acom\ Vcom^2 + 24\, t\, Acom^2\, Vcom\ D2 + 3\, t\, Acom^3\, D2^2 - 52\, Vcom^3 - 42\, Vcom^2\, D2\ Acom - 12\, Vcom\ D2^2\, Acom^2 - D2^3\, Acom^3)/(6\, Acom\ Vcom)$$

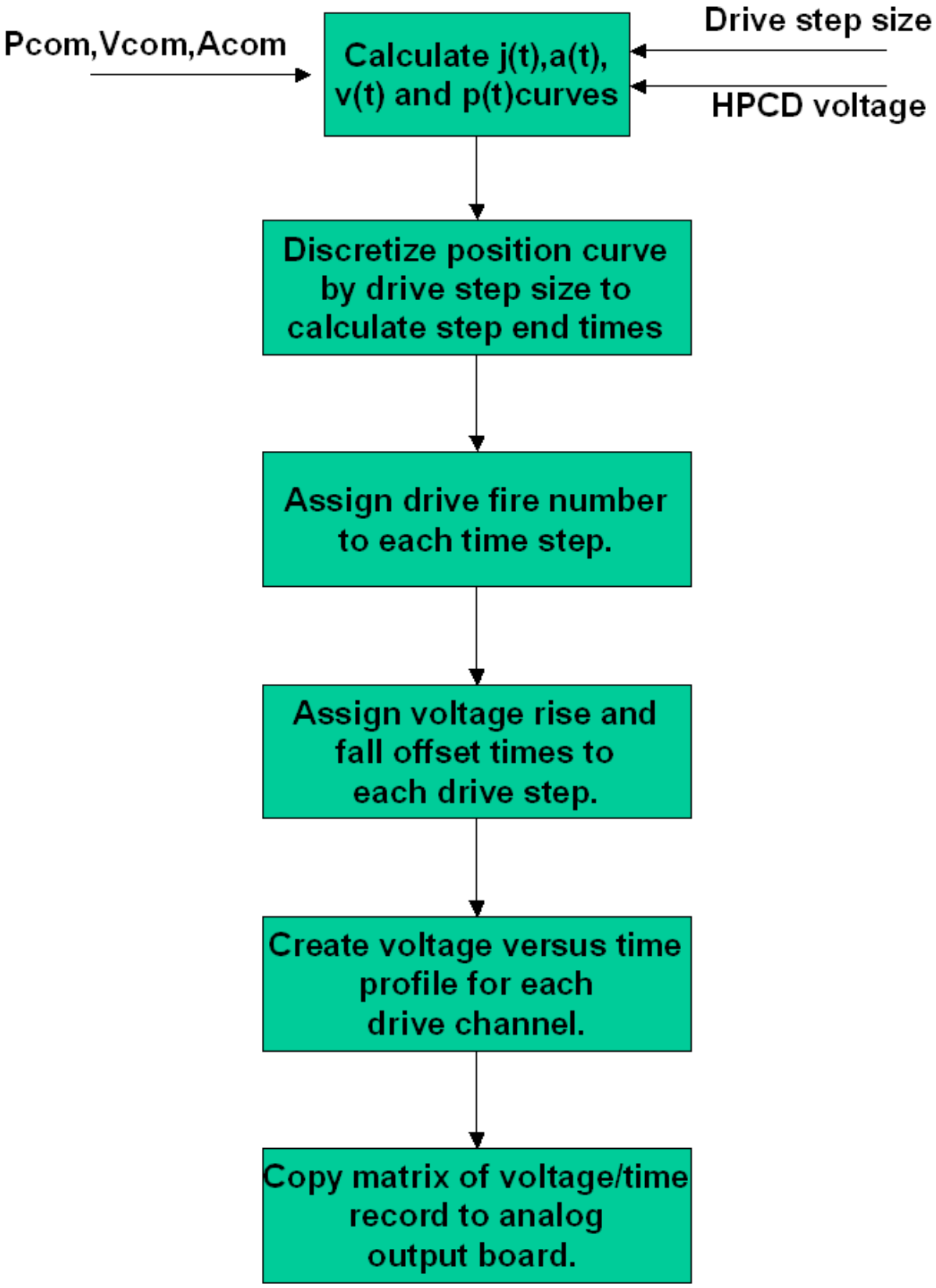

Figure 4-15 Algorithm used to calculate the time/voltage record for the LSDT motion control.

Using the MATLAB Data Acquisition Toolbox, the voltage-time record is copied to the National Instrument AT-AO-10 analog output board. Signals generated by the AT-AO-10 are amplified through a set of Sandia designed amplifiers for MEMS. The voltage signals then travel to the MEMS device on the probe station through manual probers (Figure 4-16).

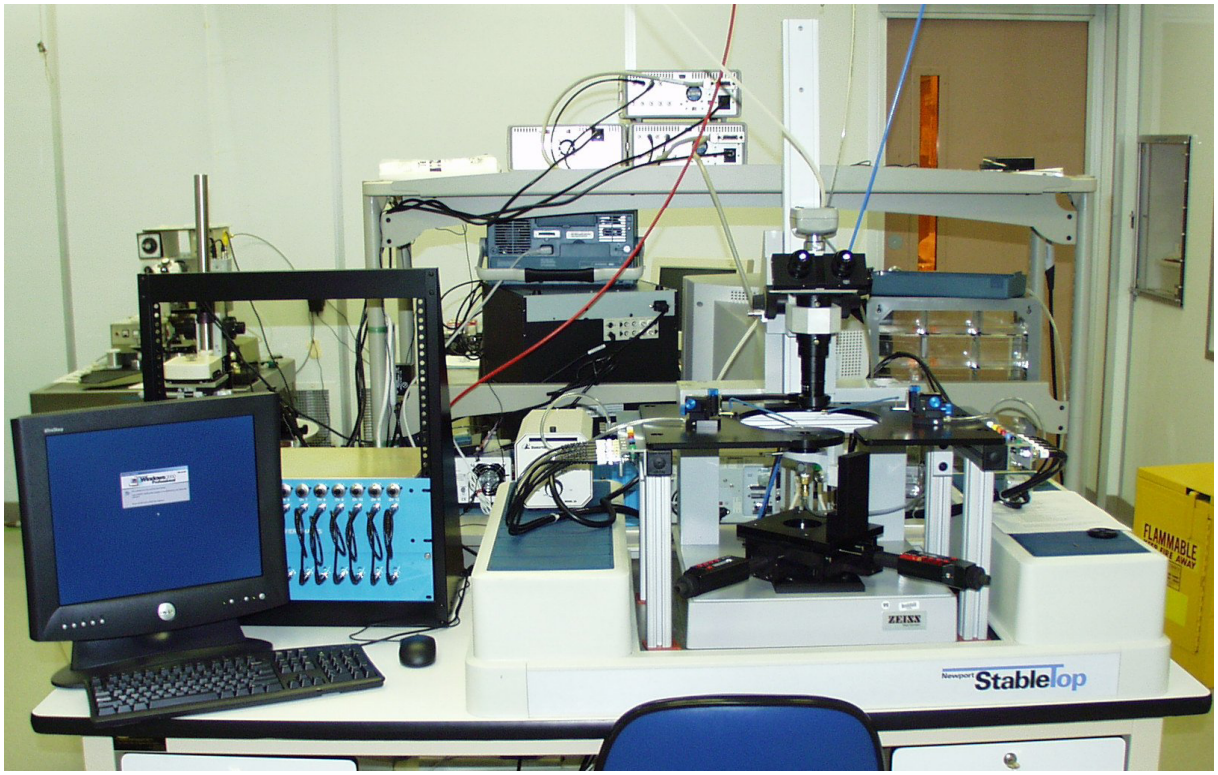

Figure 4-16 Probe station setup with computer, amplifier and probers.

4.10. Generation 3 – Force Output

Actuator output force was estimated by a fixed-fixed beam force gauge built into special versions of the track drives (Figure 4-17a). The force gauge device was calibrated through non-linear finite element analysis (FEA) (Figure 4-17b).

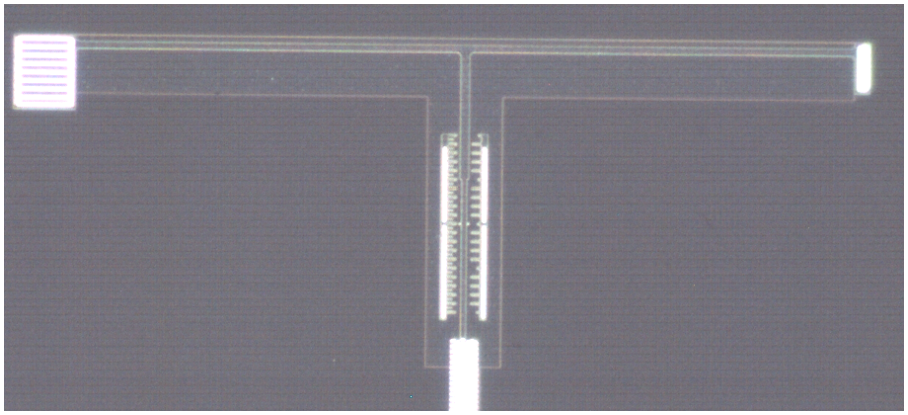

(a)

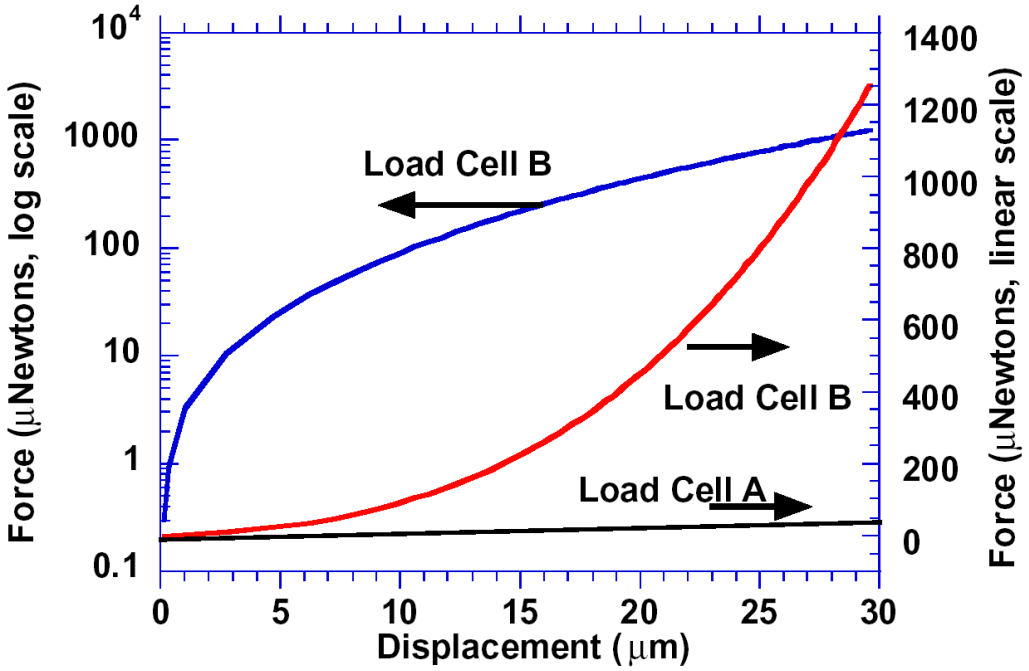

(b)

Figure 4-17 Fixed-fixed beam force gauge (a) picture of device on chip, and (b) calibration curve generated by FEA.

Using the calibration curve, the force could be estimated for each device. Results for the overall performance is shown in Table 4-4. There appeared to be little difference in force output between the single-sided and double-sided devices, allowing the results to be combined into one table.

Table 4-4 Estimated force (μN) in LSTDs.

Type			# of Comb Banks	Drive Voltage		
				40	**60**	**80**
Calculated Force Output	**Contituent Actuators**	**Low**	3	32	71	126
		Medium	4	42	95	168
		High	5	53	118	210
	LSTD with MA=0.9	**Low**	3	28	64	114
		Medium	4	38	85	151
		High	5	47	106	189
	LSTD with MA=1.3	**Low**	3	41	92	164
		Medium	4	55	123	219
		High	5	68	154	273
Verified force output				25-60	50-100	110

5. XYC Planar Motion Platform

The XYC planar motion platform was the first design created, built and tested. The "XYC" notation refers to the motion achieveable by the platform – in-plane translation in the X and Y directions and rotation about the axis normal to the fabrication plane (Z-axis) ordinarily referred to as the "C" direction. Two generations of the platform were built. The major difference between the two was the way they were actuated.

5.1. Generation 1

The Generation 1 XYC device (XYC1) was conceived of, designed and fabricated by Jim Allen, Gilbert Benavides and Lothar Bieg. XYC1 consisted of three push-pull electrostatic comb-drive actuators connected to a single platform by three jointed linkages (Figure 5-1). XYC1 was design as a demonstrator to show that planar motion control was possible in MEMS.

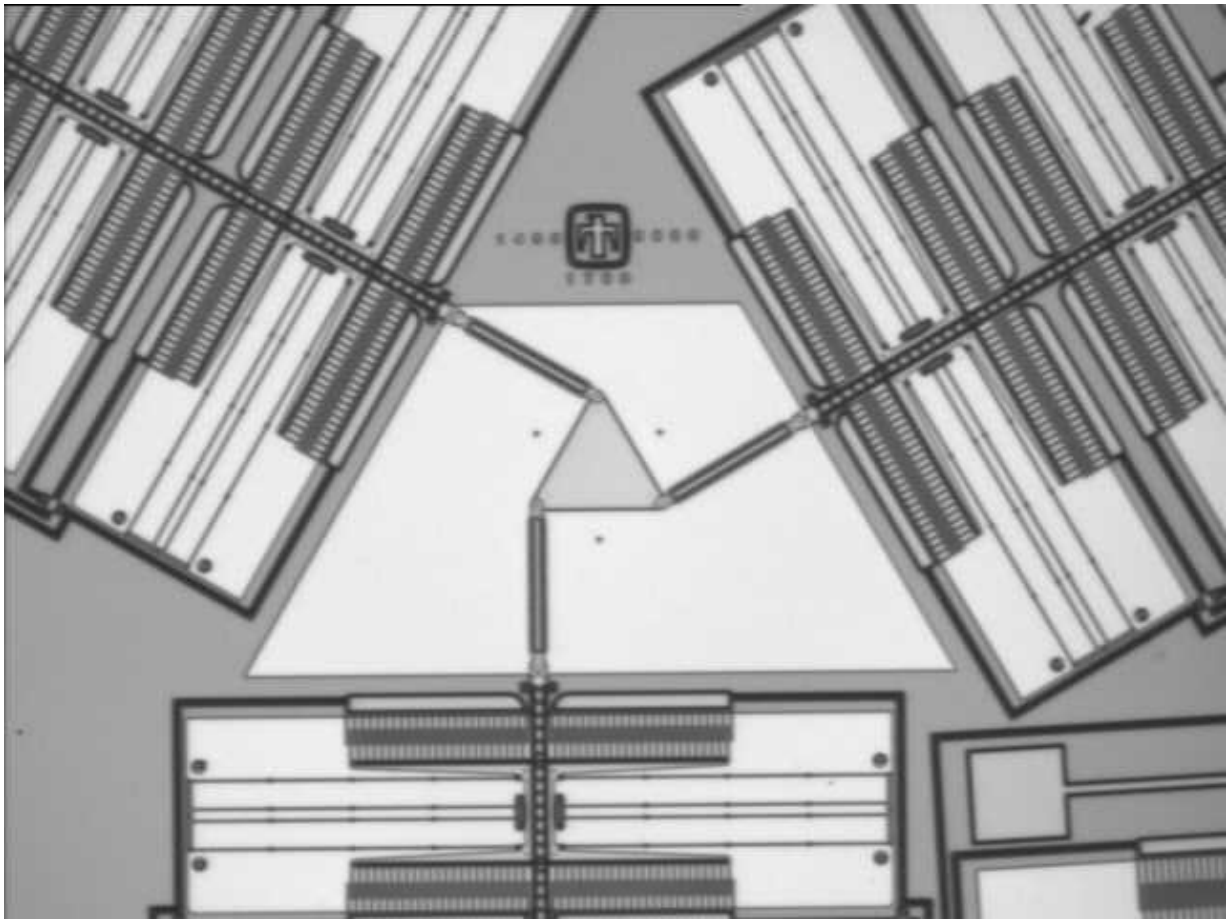

Figure 5-1 A picture of XYC1.

The comb drives were driven by time-varying voltage signals applied to each of the two banks of the three comb drives. They had an approximate stroke of ±17um, giving XYC1 a planar work volume of approximately 200μm^2.

As stated in Chapter 4 the main driving force of the project was to demonstrate position control in MEMS. The comb drives on XYC1 did not have any positional control capability (no stepping or positional feedback mechanisms). In order to make XYC1 be a position control mechanism a great deal of effort to calibrate the device under varying loads, drive voltages and velocities would have had to be done. However XYC1 was successfully tested and clearly illustrated the potential of using PKMs in MEMS to create motion control systems, but it was never intended to be fully tested and characterized for use as a robust and perfected device.

5.2. Generation 2

The Generation 2 XYC device (XYC2) was an XYC1 device with the Generation 1 linear stepping track drives (LSTD) (Figure 5-2).

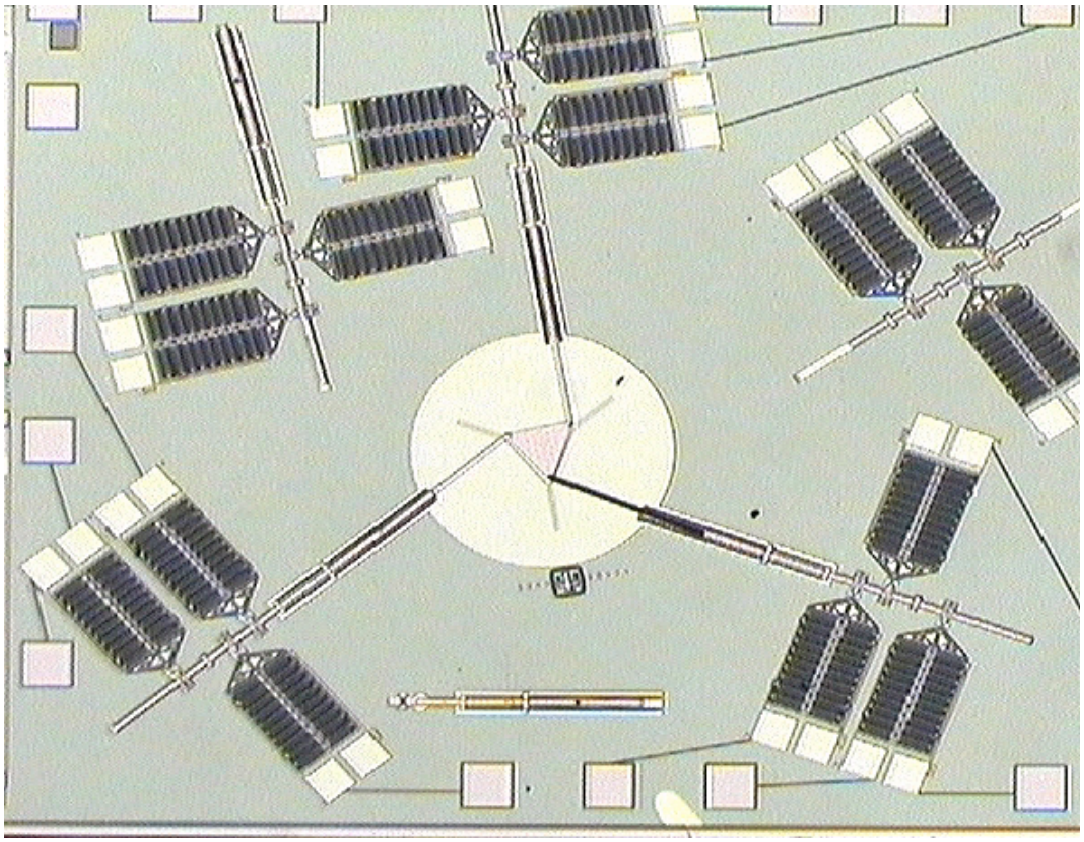

Figure 5-2 - A picture of XYC2.

XYC2 was not very successfully tested. Mainly this was due to cogging problems in the first generation LSTDs (please refer back to Chapter 4 for more information). However XYC2 was tested successfully enough to demonstrate the potential of the stepping track drive as an important and useful position control actuator in MEMS. Therefore while the particular design of XYC2 was not successful it was wildly successful in proving the point that with improved design position control in MEMS was indeed possible.

6. XYZ Translation Only Spatial Motion Platform

Once it was shown that position control in MEMS was possible, the direction of the LDRD changed to exclusively pursue spatial motion control in MEMS – in other words creating a device in silicon MEMS that could controllably move a platform in space on a chip.

6.1. Generation 1

The Generation 1 XYZ device (XYZ1) was the first attempt at demonstrating on-chip spatial motion control. It was similar to the XYC1 and XYC2 devices in that it had three linear actuators that displaced three jointed linkages connected to a platform (Figure 6-1). Generation 2 LSTDs were used exclusively in this design (again please refer to Chapter 4 for more information) over the push-pull comb drives.

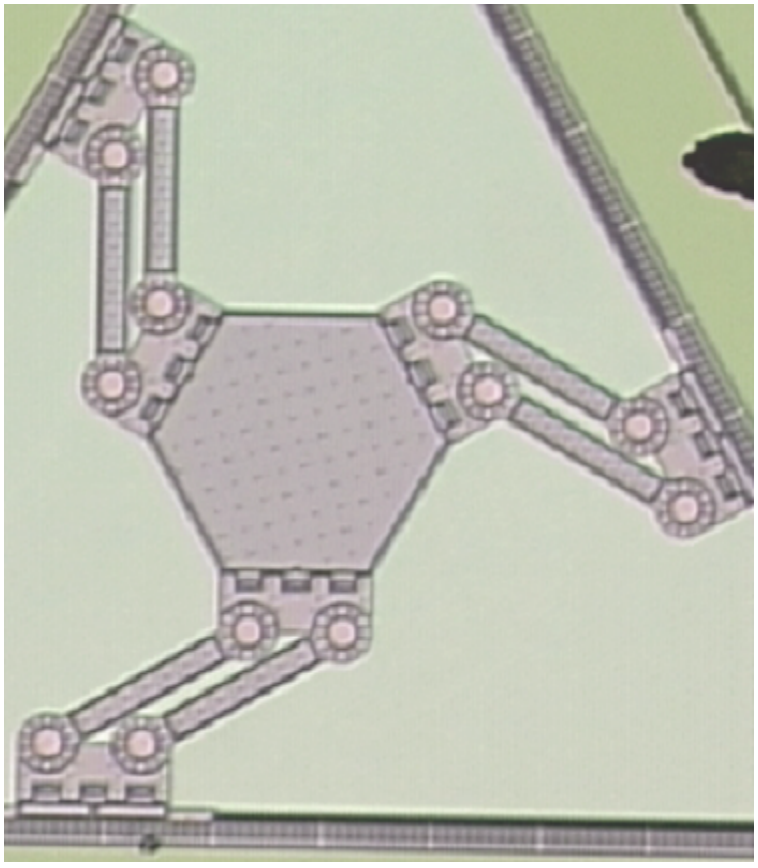

Figure 6-1 - A picture of XYZ1 in its unreleased state.

XYZ1was never tested at all. It was very unfortunate that there was a design error in the masks, which didn't allow the Poly1 rings to form correctly around the pin joints. This mistake caused the entire device to be unconstrained with respect to the substrate during release. In other words when the device went through the release process, the silicon mechanism merely floated away when the silicon dioxide dissolved. Figure 6-2 shows what was left of XYZ1 post-release.

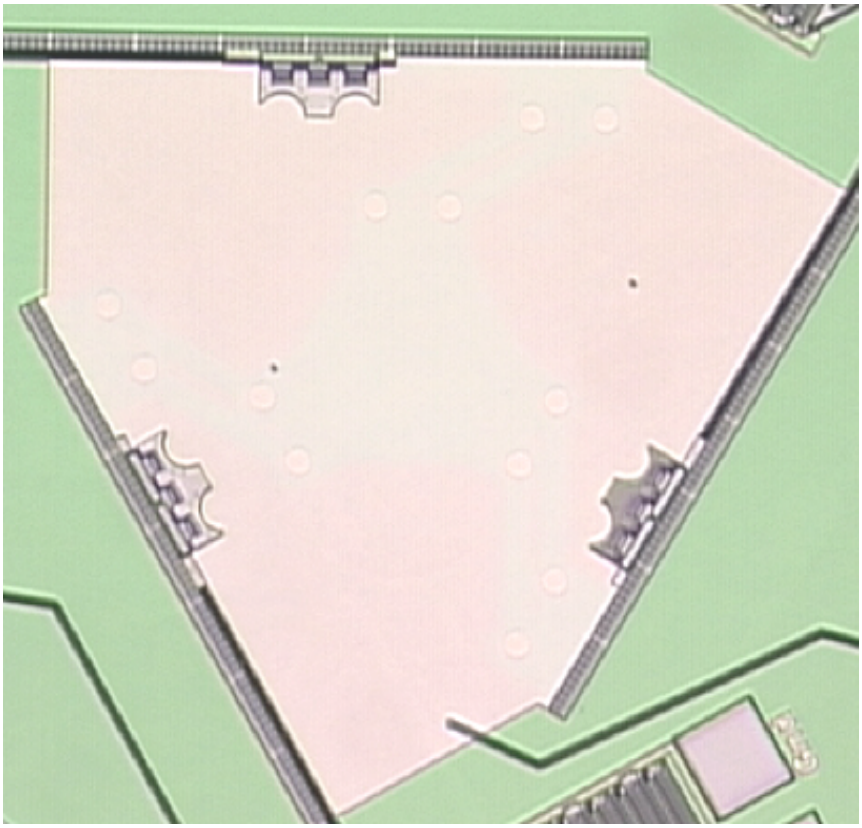

Figure 6-2 - A picture of XYZ1 after release.

The design problem in the joints was found by looking at pictured of focused-ion-beam (FIB) cuts through the joints (performed by Jeremy Walraven and Alex Pimentel). On an unreleased part the unwanted cut though the Poly1 ring in clearly visible (Figure 6-3a). However neither the design rule checker nor the solid modeling algorithm caught the mistake (Figure 6-3b).

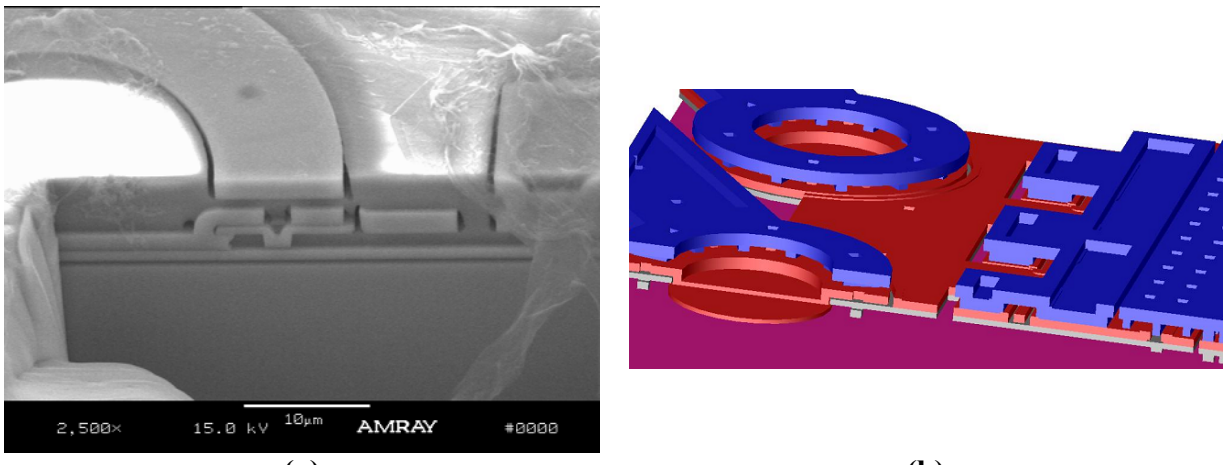

(a) **(b)**

Figure 6-3 – Evidence of XYZ2 design error (a) FIB cut thought pin joint, and (b) the corresponding cut through the computer generated solid model from the mask designs.

While the spatial motion control aspect of XYZ2 was not demonstrated, it was shown that the improved LSTD design did work and allowed the cogging problem in the LSTD to be fully debugged and corrected in future LSTD designs.

6.2. Generation 2

The second generation of the XYZ translation only platform (XYZ2) was immensely successful. Two versions of XYZ2 were incorporated on a two-module (concatenated) die along with other spatial motion designs (Figure 6-4).

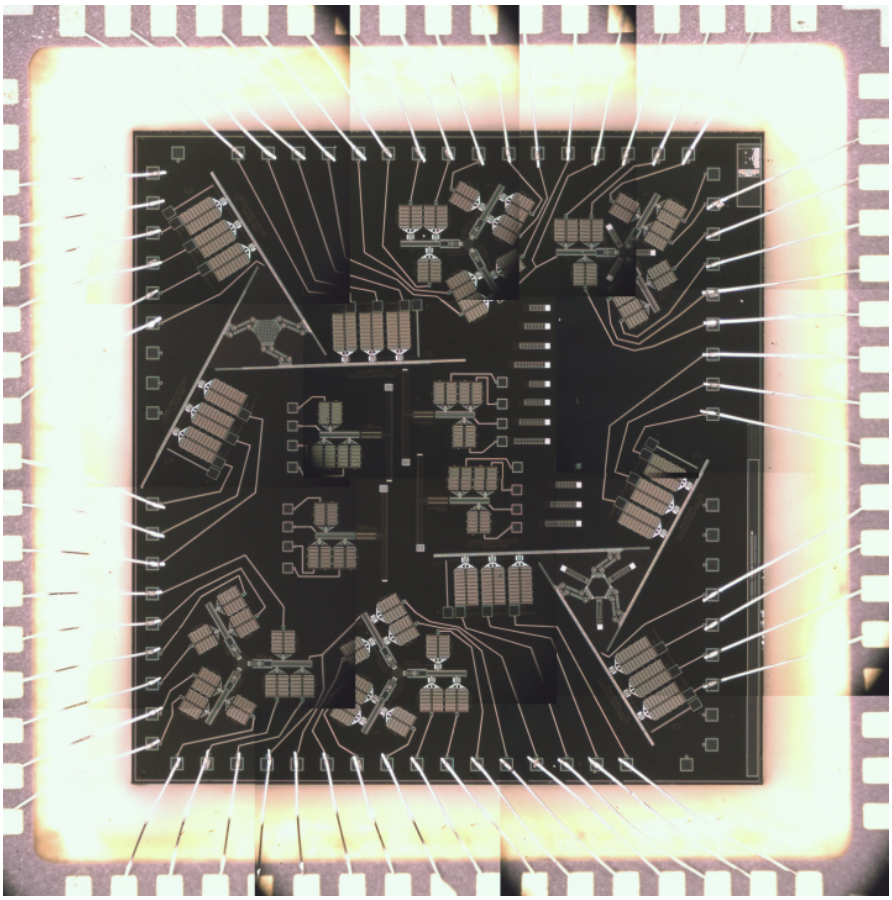

Figure 6-4 - A picture of concatenated module containing two versions of XYZ2 in its released state (XYZ2-1 upper left, XYZ2-2 lower right).

The main difference between the two designs was in the platform design. XYZ2-1 was a solid honey combed designed built to be very stiff (Figure 6-5a). XYZ2-2 had a honey combed ring-type platform (Figure 6-5b). The “fingers” that are underneath XYZ2-2 were encased oxide beams that were supposed to curl up and bias the platform out of plane. However these particular designs did not function correctly.

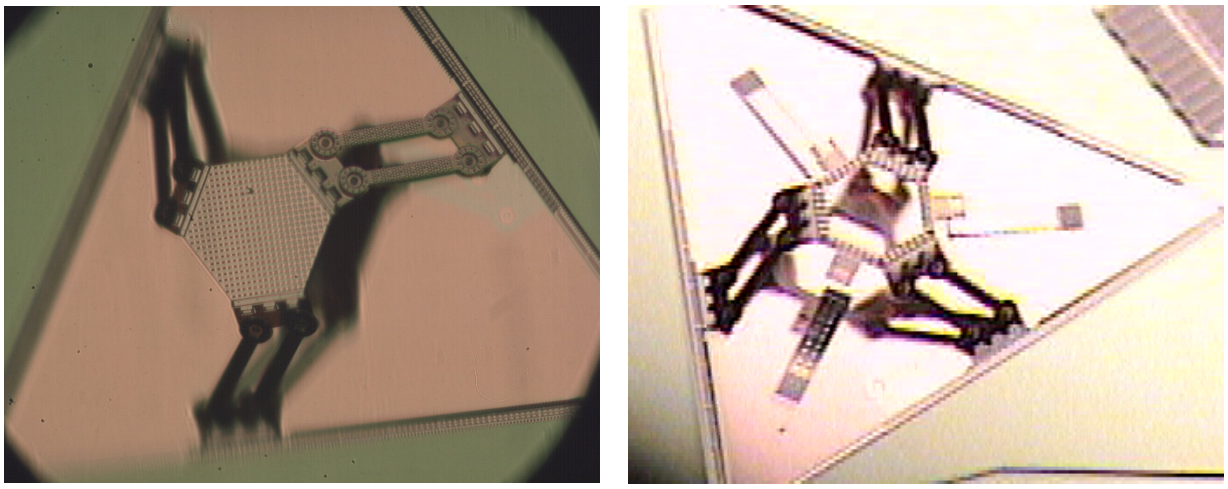

(a) **(b)**

Figure 6-5 – Two versions of XYZ2 (a) XYZ2-1 with a solid platform, and (b) XYZ2-2 with a ring platform.

Both of the designs had work volumes that could be approximated by a 50µm diameter cylinder approximately 100µm tall. However the true work volume appears in Figure 6-6.

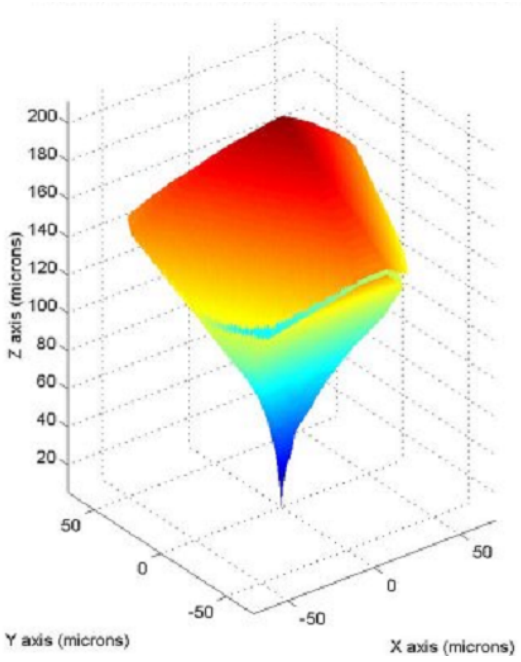

Figure 6-6 - The work volume for both XYZ2 versions.

Both versions were successfully tested. Both were biased out of plane either by manual probing or by impact biasing (turning the die package over and banging it on the table – crude but it did work) which allowed the devices to overcome initial stiction. The LSTD drives could then be engaged to drive the devices. Platform motion was achieved during testing of each device design through computer control of the LSTDs. However it was difficult to operate all three of the LSTDs at the same time.

LSTDs could be operated one at a time without difficulty, but when two or more LSTD were driven at the same time one of the LSTDs would jam. It did not appear to be a software or computer control problem. It appeared to be an actuator problem. When the XYZ2 devices move the amount of force required by the actuators to move the platform varies. This variation depends on the pose of the device, its trajectory and it velocity. It appears as though that the LSTDs that were used were not strong enough to move the platform in a full three-axis contouring mode due to the varying actuation forces required. Since the LSTDs could not produce enough force two of the constituent HPCD actuators would jam against the track effectively locking up the device. The only way to remedy this was to use a probe to physically "pop loose" one of the HPCD actuators.

This not withstanding the XYZ2 device were successfully released and tested under computer control showing absolutely that on-chip motion control was not only possible, but also a reality.

6.3. Control System

The control system for the XYZ devices was also developed. Again building on the computational and interfacing capabilities of MATLAB, a control system and graphical user interface (GUI) was created that emulated a CNC machine tool (Figure 6-7).

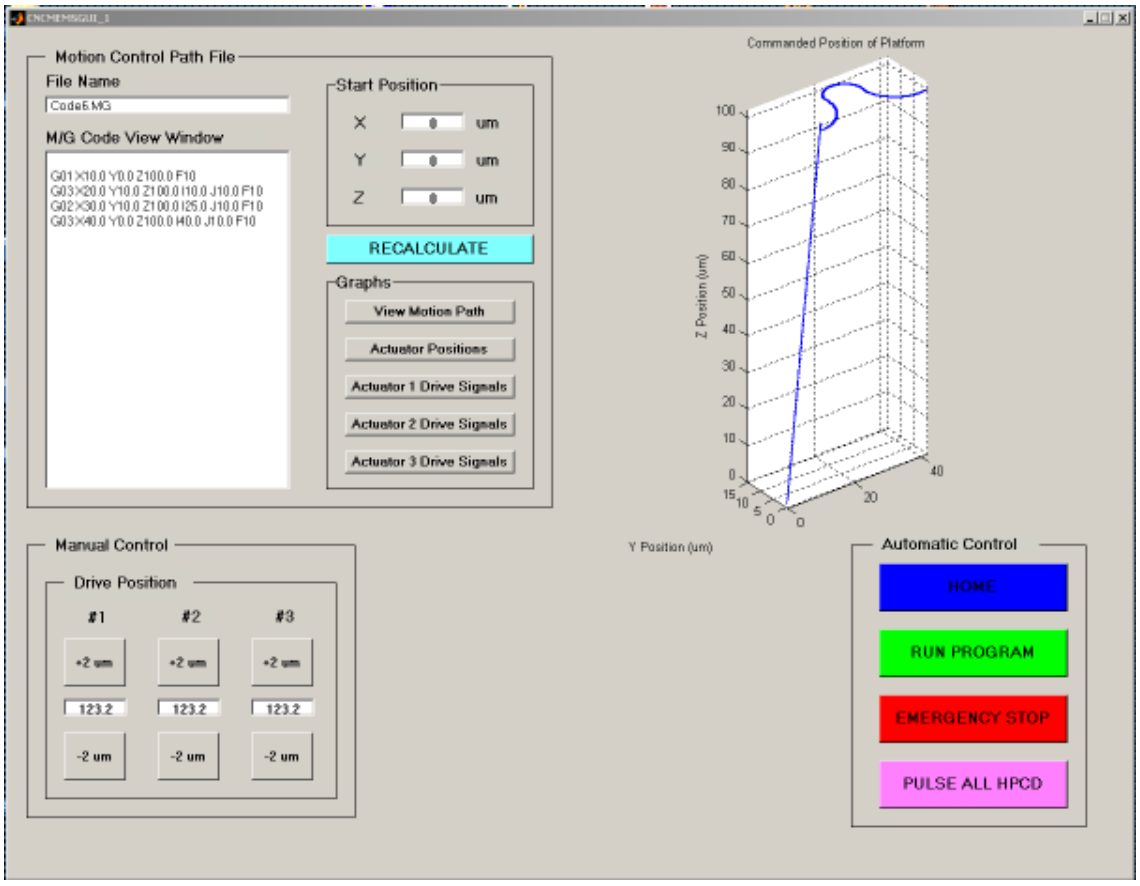

Figure 6-7 - GUI for the XYZ position control system.

The driver program decodes a M/G code (a text file used to program most CNC machine tools). The geometry from the M/G code is then interpreted and interpolated to create a list of X,Y,Z positions with their respective velocities and time steps. These XYZ coordinates and velocities are then turned into velocity trajectories for each of the three linear drives using the device reverse kinematics. The velocity trajectories are then turned into voltage-time profiles, which are used as the drive signals that are fed through the amplifier in a coordinated manner to each LSTD (Figure 6-8).

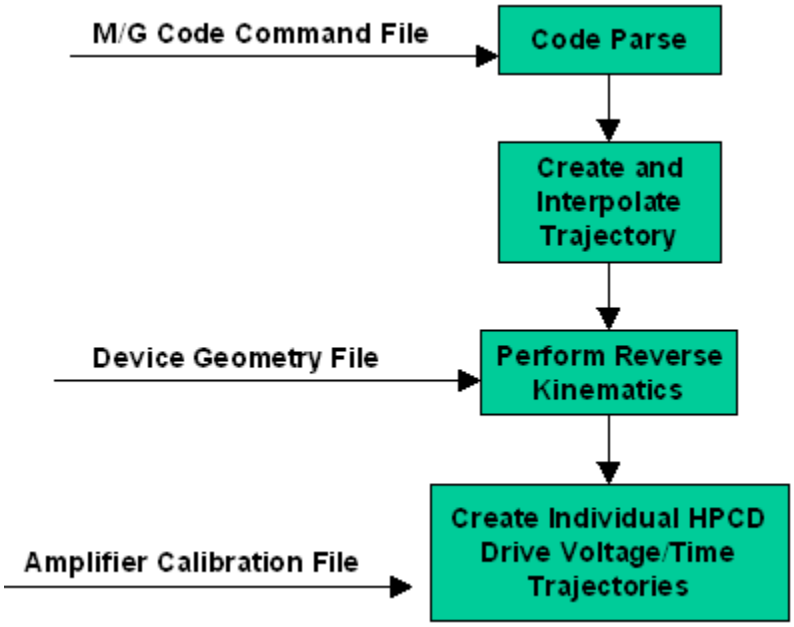

Figure 6-8 - Control system flowchart for the XYZ devices.

It is important to note that there was a significant amount of effort put into the control system that is not conveyed in this section. There is a great deal of complexity to each of the tasks in the simple-looking flowchart in Figure 6-8 that to the unaware reader is at best deceiving. Turning a set of MG code instructions into a useable set of coordinated drive signals for three LSTDs is a non-trivial task. Yet the code produced does this reliably although this report is not the place for a full explanation of the code.

7. Piston-Tip-Tilt Spatial Motion Platform

Piston-tip-tilt (PTT) motion is particularly useful for the positing of optical elements including lenses, mirrors and filters. Two generations of PTT devices were built.

7.1. Generation 1

The generation 1 PTT device (PTT1) suffered from similar design flaws that plagued XYZ1 and suffered a similar fate (Figure 7-1a and b).

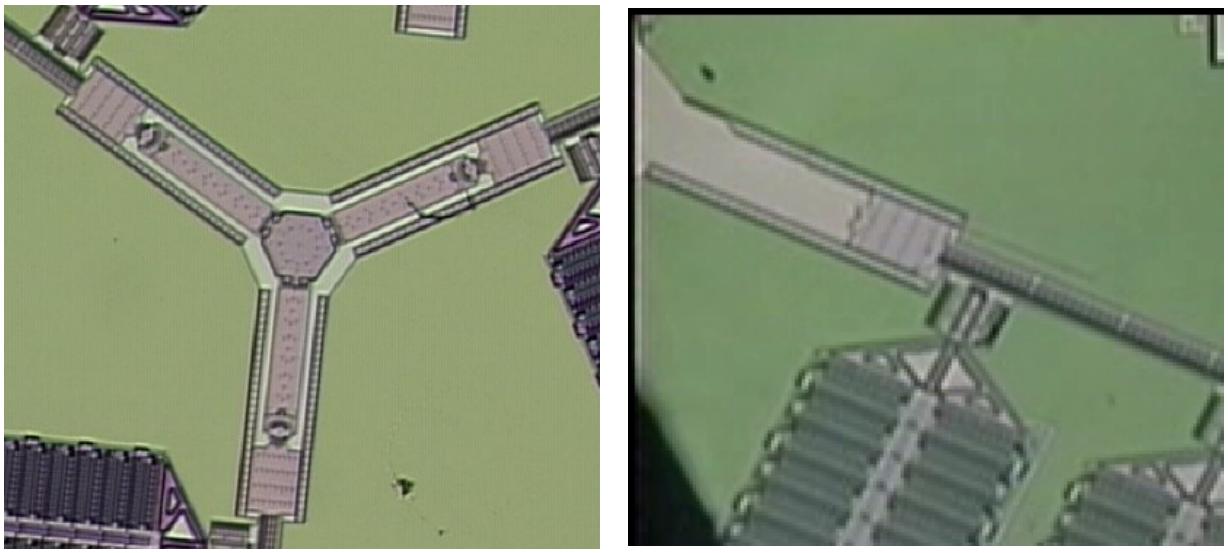

(a) **(b)**

Figure 7-1 - PTT1 (a) before release, and (b) after release.

Essentially there was nothing to test. This again was the result of the design flaw in the pin joint constraining rings. Please review section 6-1 for more information.

7.2. Generation 2

The Generation 2 PTT devices (PTT) however worked amazingly well. They were fabricated without error (no floating or missing parts). Three versions of the PTT2 were fabricated (Figure 7-2a-c).

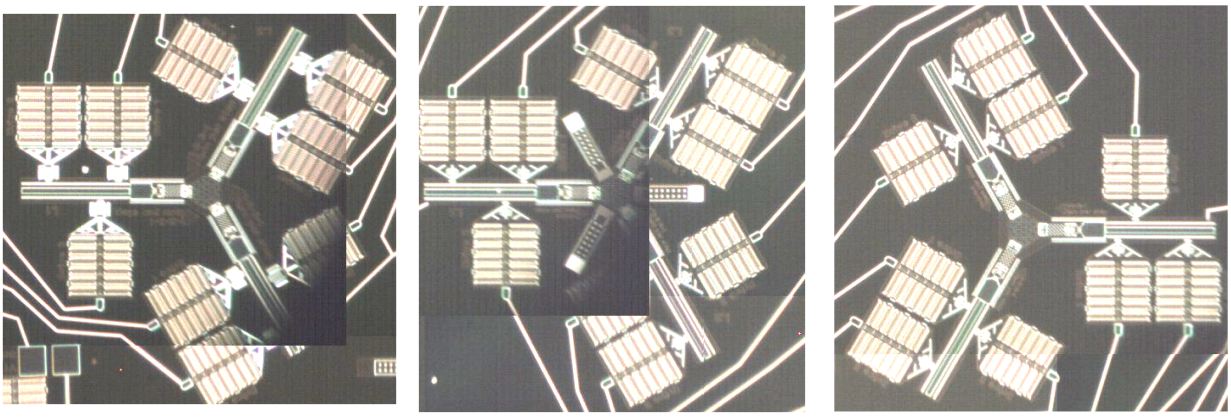

(a) (b) (c)

Figure 7-2 - Post-release pictures of the PTT2 versions (a) version 1 (PTT2-1), standard device, no vertical assist, regular double-sided LSTDs, (b) version 2 (PTT2-2), vertical assist, LSTDs with experimental HPCDs with built-in linear guides, and (c) version 3 (PTT2-3) no vertical assist, with experimental HPCD design.

All three versions could be actuated directly from their planar fabrication positions without the assistance of impact biasing or physical probing, which could not be done with the XYZ devices. This was due to two design facts. First the devices were much smaller than the XYZ devices (less stiction, less of an effect from surface effects). Second and more importantly was geometry. Due to the orientation of the LSTDs with respect to the devices the full force of the LSTDs was put directly into the structure instead of indirectly in the case of the XYZ devices. This allowed for small but large enough moment to the placed on the platform allowing it to self-erect under actuation (Figure 7-3).

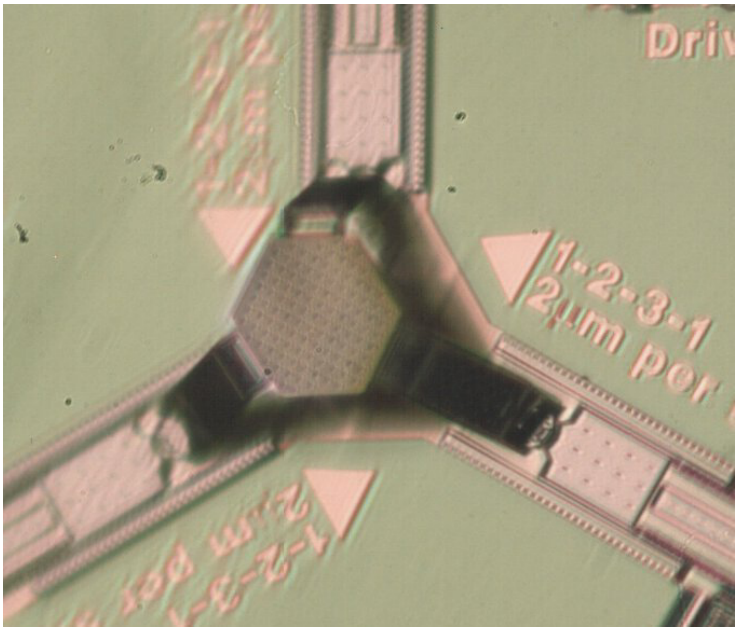

Figure 7-3 – Erected PTT2 mechanism.

7.3. Control System

Schematically the PTT devices were controlled using the same basics steps and algorithms as the XYZ (revisit Figure 6-8). However while there was a closed-form reverse solution for the XYZ devices readily available, one for the PTT devices would take a great deal more effort. Instead of getting bogged-down in trying to create a closed form solution for the PTT a look-up table method was employed instead.

A simple dimensionally correct solid model of the PTT device was created using SolidWorks (Figure 7-4).

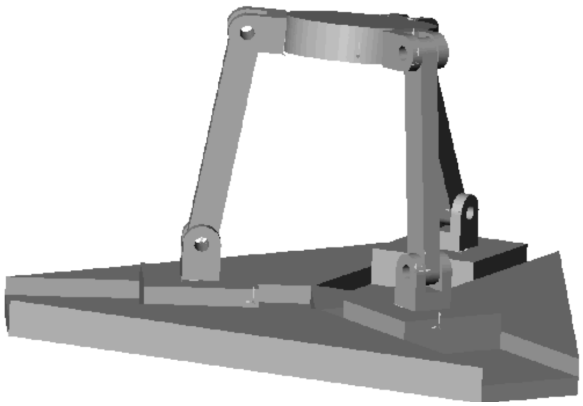

Figure 7-4 – Simplified but dimensionally accurate PTT solid model.

Using COSMOS/Motion motions were specified at each of the devices linear inputs. The software solved for the motion of the device and recorded the new position of the platform. This was repeated in minute increments until full stroke had been achieved on each linear input link. All of the record data of the platform position and orientation was then massaged by MATLAB to create three look-up tables one for each linear drive positions (Figure 7-5).

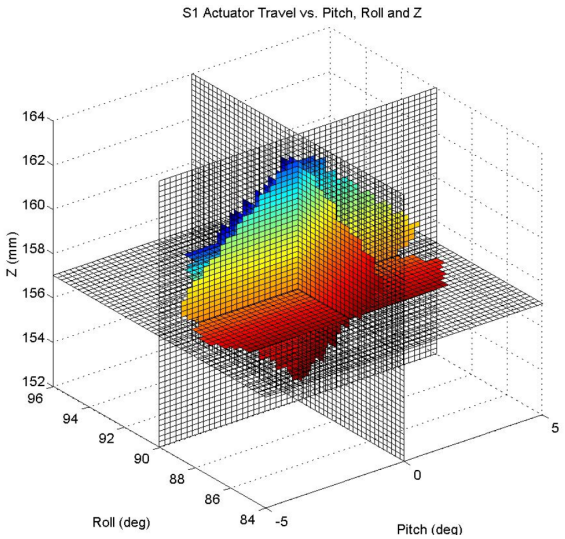

Figure 7-5 – Cut-away of the look-up table for PTT2 linear input link 1.

To use the look-up tables the user or computer algorithm would “look-up” the correct linear actuator position for each input link for the particular commanded piston (Z), tip (phi) and tilt (theta) motion specified. To get the exact or at least a very good approximation for the input link values interpolation would have to be performed.

Using the look-up table method sets of complex equations requiring iterative solution search algorithms to be solved did not have to be used. Thousands of solutions were pre-processed and stored in tables that could be interpolated over to find the correct input link commands for a given commanded platform position. This was faster, easier to implement and less resource (computer speed and memory) hungry than solving sets of equations. In testing it proved to be as transparent as the direct reverse kinematics solution as that used in the XYZ devices.

8. Conclusion

The three-year LDRD "CNC Micromachines" that was completed at the end of FY02 was undoubtedly a success. The project had four major breakthroughs in spatial motion control in MEMS.

1. A unified method for designing scalable planar and spatial on-chip motion control systems was developed. The method relies on the use of parallel kinematic mechanisms (PKMs) that when properly designed provide different types of motion on-chip without the need for post-fabrication assembly.

2. A new type of actuator was developed – the linear stepping track drive (LSTD) that provides open loop linear position control that is scalable in displacement, output force and step size. Several versions of this actuator were designed, fabricated and successfully tested.

3. Different versions of XYZ translation only and PTT motion stages were designed, successfully fabricated and successfully tested demonstrating absolutely that on-chip spatial motion control systems are not only possible, but are a reality.

4. Control algorithms, software and infrastructure based on MATLAB were created and successfully implemented to drive the XYZ and PTT motion platforms in a controlled manner. The control software is capable of reading an M/G code machine tool language file, decode the instructions and correctly calculate and apply position and velocity trajectories to the motion devices linear drive inputs to position the device platform along the trajectory as specified by the input file.

While more work is needed to perfect and harden the devices and technologies that were attempted and developed during the course of the CNC Micromachines LDRD, there is little doubt that the technology for on-chip motion control has been greatly furthered by this work. Major questions have been answered and obstacles negotiated that have stood in the way, and a strong foundation for future work and device implementation has been built.

9. Bibliography

1. Mc.Brayer, J., "Sandia's Ultra-planner Multilevel MEMS Technology", Sandia Introductory MEMS Short Course Notes, Chapter 4, pg 20, 2000.

2. Allen, J., "Summit-V Layers", Sandia MEMS Advanced Design Short Course Notes, Chapter 15, pg 3, 2000.

3. Jokiel, B., "Planar and Spatial Three-Degree-of-Freedom Microstages in Silicon MEMS", Proceedings of the 2001 ASPE Winter Annual Meeting, Crystal City, VA, pg 32.

4. de Boer, McBrayer, J., "Release Processes", Sandia Introductory MEMS Short Course Notes, Chapter 5, pg 8-10, 2000.

5. M. P. de Boer and T. M. Mayer, *Tribology of MEMS*, MRS Bull. 26 (4), 302 (2001).

6. M. P. de Boer, J. A. Knapp and P. J. Clews, *Effect of nanotexturing on interfacial adhesion in MEMS*, International Conference on Fracture, Honolulu, HI, accepted (2001).

7. *Adhesion Hysteresis of Silane Coated Microcantilevers*, M. P. de Boer, J. A. Knapp, T. A. Michalske, U. Srinivasan, R. Maboudian, *Acta mater.* 48, (18-19) 4531 (2000).

8. *The Impact of Solution Agglomeration on the Deposition of Self-Assembled Monolayers*, B.C. Bunker, R.W. Carpick, R.A. Assink, M.L. Thomas, M.G. Hankins, J.A. Voigt, D. Sipola, M.P. de Boer, G.L. Gulley, *Langmuir* 2000, *16*, 7742-7751.

9. *Supercritical Carbon Dioxide Extraction of Solvent from Micromachined Structures*, E.M. Russick, C.L.J. Adkins, C.W. Dyck.

10. *Accurate Method For Determining Adhesion of Cantilever Beams*, M. P. de Boer and T.A. Michalske, Published in the Journal of Applied Physics, July 15, 1999, Volume 86, pp. 817-827.

11. *The Role of Interfacial Properties on MEMS Performance and Reliability*, M. P. de Boer, J.A. Knapp, T.M. Mayer and T.A. Michalske, Invited paper for SPIE/EOS Conference on Microsystems Metrology and Inspection, Munich, June 15, 1999.

12. *The Effect of Humidity on the Reliability of a Surface Micromachined Microengine*, D. M. Tanner, J. A. Walraven, L. W. Irwin, M. T. Dugger, N. F. Smith, W. M. Miller, and S. L. Miller, *Proc. Of IEEE International Reliability Physics Symposium*, 1999, pp. 189-197.

13. A*dhesion, Adhesion Hysteresis and Friction in MEMS Under Controlled Humidity Ambients*, M.P. de Boer, J.A. Knapp, J.M. Redmond, T.A. Michalske, R. Maboudian, Presented at the ASME IMECE conference in Anaheim, CA, Symposium on Microscale Mechanics of Materials and Structures, Nov. 1998.

14. *A Hinged-pad Test Structure for Sliding Friction Measurement in Micromachining,* Maarten P. de Boer, Jim M. Redmond and Terry A. Michalske, Published in the SPIE Proceedings, Materials and Device Characterization in Micromachining, Santa Clara, CA, Vol. 3512, Sept. 1998, pp. 241-250.

15. *Adhesion of Polysilicon Microbeams in Controlled Humidity Ambients,* M. P. de Boer, P. J. Clews, B. K. Smith and T. A. Michalske, Presented at the Materials Research Society Proceedings, San Francisco, CA, Symposium on Microelectromechanical Structures for Materials Research, April 15-16, 1998, Vol. 518, pp. 131-136.

16. *Measuring and Modeling Electrostatic Adhesion in Micromachines,* M. P. de Boer, M. R. Tabbara, M. T. Dugger, P. J. Clews and T. A. Michalske, Presented at the Transducers 1997 Meeting, Chicago, IL, June 16-19, 1997.

17. *Improved Autoadhesion Measurement Method for Micromachined Polysilicon Beams,* Maarten P. de Boer and Terry A. Michalske, Presented at the Materials Research Society Meeting, Symposium on Materials for Mechanical and Optical Microsystems, Boston, MA, Dec. 2-3, 1996. Published in Materials Research Society Proceedings, Vol. 444, pp. 87-92.

18. *Failure Analysis of Surface-Micromachined Microengines,* Kenneth A. Peterson, Paiboon Tangyunyong, and Alejandro A. Pimentel, (Invited presentation and paper), Presented at the Materials and Device Characterization in Micromachining Symposium, Santa Clara, CA, September 21-22, 1998, Vol. 3512, pp. 190-200.

19. *Linkage Design Effect on the Reliability of Surface Micromachined Microengines Driving a Load,* Danelle M. Tanner, Kenneth A. Peterson, Lloyd W. Irwin, Paiboon Tangyunyong, William M. Miller, William P. Eaton, Norman F. Smith, and M. Steven Rodgers, Presented at the Micromachining and Microfabrication Symposium, September, 21-22, 1998, Santa Clara, CA, Proceedings of SPIE, Vol. 3512, pp. 215-226.

20. *MEMS Reliability: The Challenge and the Promise,* William M. Miller, Danelle M. Tanner, Samuel L. Miller, Kenneth A. Peterson, (Invited presentation and paper) 4th Annual "The Reliability Challenge," Dublin, Ireland, May 19, 1998, pp. 4.1-4.7.

21. *Failure Modes in Surface Micromachined MicroElectroMechanical Actuators,* S. L. Miller, M. S. Rodgers, G. LaVigne, J. J. Sniegowski, P. Clews, D. M. Tanner, and K. A. Peterson, Presented at the 1998 IEEE International Reliability Physics Symposium Proceedings, IRPS 1998, March 31-April 2, 1998, pp. 17-25.

22. *Dynamic Effects of Linkage Joints in Electrostatic Microengines,* J. J. Allen, S. L. Miller, G. F. LaVigne, M. S. Rodgers, Presented at Modeling and Simulation of Microsystems 1998, Santa Clara, CA, April 6-8, 1998.

23. *First Reliability Test of a Surface Micromachined Microengine Using SHiMMeR*, D. M. Tanner, N. F. Smith, D. J. Bowman. W. P. Eaton, and K. A Peterson, Presented at the 1997

Symposium on Micromachining and Microfabrication, September 29, Austin, TX. Proceedings of SPIE, Volume 3224, pp. 14-23, 1997.

24. *Routes to failure in rotating MEMS devices experiencing sliding friction*, S. L. Miller, G. LaVigne, M. S. Rodgers, J. J. Sniegowski, J. P. Waters, and P. J. McWhorter, Proc. SPIE Micromachined Devices and Components III Vol. 3324, Austin, Sept. 29-30, 1997, pp. 24-30.

25. *Characterization of Electrothermal Actuators and Arrays Fabricated in a Four-Level, Planarized Surface-Micromachined Polycrystalline Silicon Process*, J. H. Comtois, M. A. Michalicek, and C. C. Baron, (Invited Paper) 1997 International Conference on Solid-State Sensors and Actuators, Chicago, IL, June 16-19, 1997, Vol. 2, pp. 769-772.

26. *Friction in Surface Micromachined Microengines*, S. L. Miller, J. J. Sniegowski, G. LaVigne, and P. J. McWhorter, Proc. SPIE Smart Electronics and MEMS Vol. 2722, San Diego, Feb. 28-29, 1996, pp. 197-204.

27. *Release-etch modeling for complex surface micromachined structures*, W.P. Eaton, J.H. Smith, and R.L. Jarecki, Micromachining and Microfabrication Symposium, Proceedings of the SPIE, Vol 2879, pp. 80-93 (October 1996).

28. *Supercritical Carbon Dioxide Drying of Surface-Micromachined Micromechanical Structures,* C. Dyck, J. Smith, E. Russick, and C. Adkins, SPIE vol. 2879, Oct. 1996.

29. Yeh, R., Pister, K.S., "Measurement of static friction in mechanical couplings of articulated microrobots", SPIE Symposium on Micromachining and Microfabrication, Austin Texas, October 23-24, 1995.

30. Statics and Kinematics with Applications to Robotics,Duffy, J., Cambridge University Press, 1996.

31. Parallel Robots, Merlet, J., Kluwer Academic Publishers, 2000.

10. Distribution List

# Copies	Mail Stop (MS)	Recipient
1	0329	Kelly Klody, 2614
1	0523	Lothar Bieg, 1733
1	0958	Alan Parker, 14184
1	0958	Gilbert Benavides, 14184
1	0958	Ed Wyckoff, 14184
1	0961	Carol Adkins, 14100
1	1076	Thom Fischer, 1745
1	1076	Bernhard Jokiel, 1745
1	1080	David Sandison, 1769
1	1080	Jim Allen, 1769
1	9018	Central Technical Files, 8945-1
2	0899	Technical Library, 9616
1	0612	Review and Approval Desk, 9612,